Czech Technical University in Prague

Faculty of Mechanical Engineering

Department of Mechanics, Biomechanics and Mechatronics

Thesis

Action potential in a biomechanical view

by Bc. David Vodička
supervisor prof. RNDr. Matej Daniel, Ph.D
Prague, 2021

ZADÁNÍ DIPLOMOVÉ PRÁCE

I. OSOBNÍ A STUDIJNÍ ÚDAJE

Příjmení: **Vodička** Jméno: **David** Osobní číslo: **467319**

Fakulta/ústav: **Fakulta strojní**

Zadávající katedra/ústav: **Ústav mechaniky, biomechaniky a mechatroniky**

Studijní program: **Aplikované vědy ve strojním inženýrství**

Specializace: **Biomechanika**

II. ÚDAJE K DIPLOMOVÉ PRÁCI

Název diplomové práce:

Akční potenciál z pohledu biomechaniky

Název diplomové práce anglicky:

Action potential in a biomechanical view

Pokyny pro vypracování:

1. Hodghin-Huxleyho model
2. Formulace mechaniky otevření iontových kanálů
3. Experimentální důkaz

Seznam doporučené literatury:

Hodgkin, A L, and A F Huxley. “A Quantitative Description of Membrane Current and Its Application to Conduction and Excitation in Nerve.” J. Physiol. 117, no. 4 (August 1952): 500–544. https://doi.org/10.1113/jphysiol.1952.sp004764.
Heimburg, Thomas. “Thermal Biophysics of Membranes.” In Therm. Biophys. Membr., 1–361. Wiley-VCH Verlag GmbH, 2007. https://doi.org/10.1002/9783527611591.

Jméno a pracoviště vedoucí(ho) diplomové práce:

prof. RNDr. Matej Daniel, Ph.D., České vysoké učení technické v Praze, Fakulta strojní

Jméno a pracoviště druhé(ho) vedoucí(ho) nebo konzultanta(ky) diplomové práce:

Datum zadání diplomové práce: **12.04.2021** Termín odevzdání diplomové práce: **13.08.2021**

Platnost zadání diplomové práce: _____

prof. RNDr. Matej Daniel, Ph.D.	doc. Ing. Miroslav Španiel, CSc.	prof. Ing. Michael Valášek, DrSc.
podpis vedoucí(ho) práce	podpis vedoucí(ho) ústavu/katedry	podpis děkana(ky)

III. PŘEVZETÍ ZADÁNÍ

Diplomant bere na vědomí, že je povinen vypracovat diplomovou práci samostatně, bez cizí pomoci, s výjimkou poskytnutých konzultací. Seznam použité literatury, jiných pramenů a jmen konzultantů je třeba uvést v diplomové práci.

. _____ _____

Datum převzetí zadání Podpis studenta

Abstract

Most used model at this time, the Hodgkin-Huxley model for describing action potential, deals only with electrical properties of nerve impulse. It was experimentally proved action potential is coupled with a number of nonelectric phenomena, such as the change of axon thickness and length, reabsorption of released heat or change in optical properties. Many models for the origin and propagation of action potential were created. None of the present models explicitly incorporates the mechanical properties of the excitable membrane. In this thesis a viscoelastic model is derived which can explain the opening and closing of ion channels and therefore the mechanism of inducing the action potential. This model was successfully fitted to the original data of Hodgkin and Huxley, 1952. A unique experiment was conducted with mice neurons and the use of an atomic force microscope. Compared to other experiments this measurement was done using spontaneous action potentials. This means the nerve impulse is not electrically evoked, but one waits until the impulse occurs spontaneously. This ensures the action potential is not altered in any way by the measurement. The experiment has proved existing relationship between the change of the axon diameter and the action potential.

Keywords

Action potential, Viscoelasticity, Atomic force microscopy, Hodgkin-Huxley model of nerve impulse

Abstrakt

Nejvíce užívaný model pro popis akčního potenciálu v tuto chvíli, Hodgkin-Huxleyho model, pracuje pouze s elektrickými vlastnostmi nervového impulsu. Experimentálně bylo prokázáno, že akční potenciál je spojen s množstvím neelektrických dějů, jako například změna tloušťky a délky axonu, reabsorbce uvolněného tepla či změna optických vlastností. Pro popis vzniku a šíření akčního potenciálu bylo vytvořeno mnoho modelů. Žádný z dosavadních modelů ale explicitně nezahrnuje mechanické vlastnosti vzrušivé membrány. V této diplomové práci byl odvozen viskoelastický model, kterým je možné vysvětlit chování iontových kanálků, jež jsou základem pro vznik akčního potenciálu. Tento model byl úspěšně nafitován na původní data Hodkinga a Huxleyho, 1952. Dále bylo ověřeno propojení akčního potenciálu s deformací membrány. Byl proveden jedinečný experiment na myších neuronech pomocí mikroskopu atomárních sil. Oproti jiným experimentům bylo toto měření provedeno se spontánními akčními potenciály. To znamená, že nervový impuls není uměle vyvolán, ale čeká se, až proběhne spontánní impuls. Výsledkem je, že nervový impuls nebyl měřením nijak pozměněn. Experiment potvrdil, že existuje vazba mezi změnou tloušťky axonu a akčním potenciálem.

Klíčová slova

Akční potenciál, Viskoelasticita, Mikroskop atomárních sil, Hodgkin-Huxleyho model nervového vzruchu

Declaration

I hereby declare this thesis represents my own work and has not been included in a thesis or dissertation submitted to Czech Technical University in Prague or any other institution for a degree, diploma or other qualifications. Wherever contributions of others are involved, every effort is made to indicate this clearly, with due reference to the literature, and acknowledgement of collaborative research and discussions.

Prague, 10.08.2021

Author's signature

Acknowledgement

I would like to thank my supervisor prof. Daniel for giving me the opportunity to participate on such a unique topic. It was a pleasant time discussing the possible solutions to this challenging problem. I would also like to thank Martin Otahal, Ph.D who let me take part in the Atomic force microscopy measurement and to people from the Institute of Experimental Medicine for preparing the cells and measuring the electrical impulses. I would like to thank my family for supporting me during my studies and encouraging me during writing of this thesis.

List of abbreviations

AFM	Atomic force microscopy
GFP	Green fluorescent protein
DIV	Day in vitro

List of symbols

a	$[Pa/V]$	conversion factor between stress and voltage
α_i	$[ms^{-1}]$	transfer rate constant
b	$[m\Omega^{-1/3} \cdot cm^{-2/3}]$	conversion factor between deformation and conductance
β_i	$[ms^{-1}]$	transfer rate constant
C_m	$[\mu F \cdot cm^{-2}]$	membrane conductance
E_i	$[mPa]$	elasticity of *ith* element
$\mathcal{E}$	$[mV]$	membrane actual potential
$\mathcal{E}_r$	$[mV]$	membrane resting potential
$\mathcal{E}_i$	$[mV]$	equilibrium potential for *ith* ion
ϵ	$[-]$	mechanical deformation
ϵ_{ch}	$[-]$	mechanical deformation of ion channel
$\dot{\epsilon}$	$[s^{-1}]$	time derivative of mechanical deformation
$\ddot{\epsilon}$	$[s^{-1}]$	second time derivative of mechanical deformation
η_i	$[mPa \cdot s]$	viscosity of *ith* element
g_i	$[m\Omega^{-1} \cdot cm^{-2}]$	conductance of *ith* ion
$\overline{g}_i$	$[m\Omega^{-1} \cdot cm^{-2}]$	constant for conductance of *ith* ion
h	$[-]$	proportion of inactivating molecules
I	$[\mu A]$	membrane current
I_i	$[\mu A]$	ion current of *ith* ion
l	$[mm]$	radius of axon
m	$[-]$	proportion of activating molecules
n	$[-]$	proportion of potassium particles inside membrane
R_m	$[m\Omega]$	membrane resistance
R_a	$[m\Omega]$	resistance of the axoplasm
σ	$[mPa]$	mechanical stress
$\dot{\sigma}$	$[mPa \cdot s^{-1}]$	time derivative of mechanical stress
V_m	$[mV]$	displacement of actual potential from resting potential
V_i	$[mV]$	displacement of *ith* ion potential from resting potential
x	$[mm]$	position along the axon axis

Contents

List of Figures

List of Tables

Chapter 1

Introduction

1.1 Overview

This thesis deals with the action potential from a biomechanical view. Examining the function of neural system and specifically the behavior of transmitting information in neural tissue stays rather domain of neurosciences. However, neuroscience is not accustomed for describing the mechanical properties of such materials. This is the reason to include other parts of science in the research of neural system. Recent experiments indicate that the conventional model, considering only electrophysiological properties of a passive membrane, might be incomplete [1]. There is a growing evidence, that the action potential is accompanied by several non-electrical phenomena. Briefly, it was shown that rapid changes in the diameter of an axon take place when an action potential progresses along the neuronal axon. Another mechanical change during an AP was confirmed by an interesting study, in which the pressure increase inside the axon was observed and can be as high as 10mPa [2]. The idea of measuring mechanical changes with atomic force microscopy during action potential is not radically new. In one experiment nerve cells were measured from the mouse neurohypophysis by AFM. It was found out that action potentials are accompanied by a movement of the surface of axon in the nanometer scale [3]. It turns out that mechanical impulses are present in variety of excitable cells. For example an experiment with the plants of the Chara species showed that action potentials were followed by a deflection of the surface of a cell. These plants are capable of producing action potentials thanks to excitable plant cells. The deflection of the surface was recorded by video microscopy [4].

These phenomena cannot be attributed solely to an electrical signal, on the contrary they are likely to play an important role in the propagation and processing of the signal within the neural cell by themselves. Mechanics plays a significant role in nervous system development and in maintaining homeostasis. For a long time the explanations of brain functioning were mainly electrical and biochemical. Currently, it is known that cells are able to perceive the changes in osmotic pressure or shear forces and adapt to these changes. The coupling of mechanics and biochemistry might better explain things such as recovering after brain injuries [5].

The first chapter provides an introduction to membrane functioning and essential electrical aspects of action potential. The second chapter describes various methods for measuring electrical and mechanical properties of a neuron during action potential. The third chapter states the goals of this work. The fourth chapter deals with developing a viscoelastic model for ion channels and describes the AFM measurement, how it works and

how it was used for measuring mouse neural tissue. The fifth chapter presents the results from AFM measurement. The last chapter is a discussion about the results from the AFM measurement and numerical analysis of viscoelastic models.

1.2 Description of nerve impulse

The nerve impulse is a phenomenon responsible for encoding and transmitting information in the nervous system and is also commonly called the action potential. Scientists sometimes make distinction between these two terms. The action potential is used to describe the purely electrical representation of the nerve impulse while the term nerve impulse is used for general description of what is happening in the cell during excitation. This includes mechanical, thermodynamical and optical aspects of this phenomenon. The key function in signal generation and propagation is attributed to excitable cell membrane. The membrane is able to change its permeability rapidly as a response to a change in membrane potential [6]. Conventional models consider the membrane lipids as passive electrical insulators while ion conductance is attributed exclusively to proteins of a particular class (ion channels). This view comes from impressive work of Hodgkin, Huxley and Katz, 1949 who demonstrated that the membrane conductance is voltage dependent and were able to observe that the membrane was mainly selective to sodium and potassium ions [7]. The empirical description of the sodium and the potassium conductances allowed them to set up a system of equations that predict the action potential time course and all the properties of excitability such as threshold, refractory period, fluxes, etc [7]. The pulse propagation was predicted by combining these equations with the cable properties of the axon. This idea is expressed in the Hodgkin-Huxley model.

The primary ions in the action potential are sodium and potassium ions although other ions such as calcium or chloride ions are present in the process too. The membrane potential is defined as a difference between the potential on the inner side of the membrane and the potential on the outer side of the membrane. The resting membrane potential is a state of the cell membrane when no net flow of electrical current across the membrane is present [6]. An action potential is a dynamic process which has few distinct phases. First the membrane is rapidly depolarized. This phase ends with a peak potential where the value of membrane potential is positive. The potential then declines to a value which is lower than the initial resting potential. This phase is also called the repolarization. The last phase is the refractory period, also called hyperpolarization. During this phase the membrane potential is slowly climbing to the resting potential [6].

1.3 Membrane potential

In 1912 Bernstein came up with the hypothesis that resting membrane potential is caused by selective permeability of membrane to potassium ions [9]. He was not aware of the lipid bilayer structure of cellular membranes or ion channels as these things were discovered later, yet his hypothesis was proven right. It is caused by the membrane higher selective permeability to potassium ions over other ions. The intracellular space consists of negatively charged organic ions and positively charged potassium ions. The extracellular space consists mainly of positively charged calcium ions. The intracellular concentration of potassium ions is much greater than the extracellular concentration, which means potassium ions will tend to exit the membrane thanks to diffusion. But the movement of positively charged potassium ions means that the intracellular space becomes negatively charged. As the membrane does not permit positively charged calcium ions to enter the

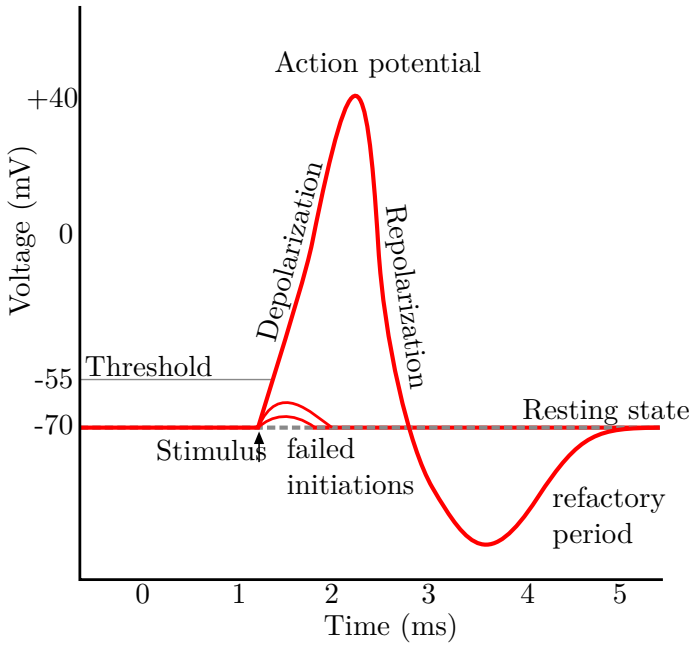

Figure 1.1: Schematic of action potential. Figure adopted from [8].

membrane, the electrochemical gradient drives the potassium ions back to the intracellular space. At equilibrium the rate at which ions leave the cell because of diffusion is equal to the rate at which ions enter the cell because of the electrochemical gradient. This is called the equilibrium potential for the given type of ion. If the membrane was permeable only to potassium ions, then the resting membrane potential would be equal to equilibrium potential of these ions. The membrane is also to some degree permeable to other ions. This results in the membrane potential being around -75mV and not exactly -92mV, as it would be in the case of a membrane permeable only to potassium ions. If something did not maintain the ionic concentration gradients, the resting membrane potential would dissipate. The sodium-potassium pump prevents this and maintains the ionic differences across the membrane by actively transporting potassium and sodium ions against their electrochemical gradients. This keeps the concentration gradient and by that the resting membrane potential [6].

In 1949 Hodgkin and Katz established another hypothesis, the so-called sodium hypothesis [10]. As opposed to Bernstein's hypothesis about resting membrane potential, the sodium hypothesis addresses the changes in the membrane potential during cell's excitation. They discovered that the amplitude of action potential decreases when the extracellular concentration of sodium ions is lowered and so they suggested that this was caused by increased permeability of sodium ions at the peak of the action potential.

1.4 Hodgkin-Huxley model

Hodgkin and Huxley compared the cell to an electrical circuit. But they were not the first ones to do so. In 1907 Lapicque came up with a model of action potential described by a simple electrical circuit. This circuit consists of a parallel capacitor and resistor. These components represent capacitance and leakage resistance of the membrane. This circuit itself cannot generate action potential. Lapicque said that the action potential was

generated when the capacitor was charged to a threshold potential. As the action potential is generated, the capacitor is discharged. This model does not care about underlying physical principles. It can, to some degree, explain the experimental results and it is used for its simplicity. Today several variants exist of this basic model addressing various issues in measured data, Adaptive integrate-and-fire or Exponential integrate-and-fire to name few. The equation 1.1 is the basic Leaky integrate-and-fire model. The I is an electric current, C_m is a membrane conductance, V_m is a membrane potential and R_m is a membrane leakage resistance [11].

$$I = C_m \frac{\mathrm{d}V_m(t)}{\mathrm{d}t} + \frac{V_m}{R_m} \tag{1.1}$$

When introducing his model of action potential, Lapicque was unaware of the potassium and sodium hypothesis. Hodgkin and Huxley decided to model the action potential in the same way as Lapicque, as an electrical circuit. They proposed an idea that the cell membrane is acting as capacitor with ion channels responsible for exchanging ions between intracellular and extracellular space. These ion channels are modelled as resistors. The ion current is then calculated as conductance times the difference between actual membrane and equilibrium potential for a given ion. For potassium ions this can be written as $I_K = g_K(\mathcal{E} - \mathcal{E}_K)$, where $\mathcal{E}_K$ is a equilibrium potential for potassium ions. It is then suitable to define ionic currents in the terms of voltages as $I_K = g_K(V - V_K)$, where $V = \mathcal{E} - \mathcal{E}_r$ and $V_K = \mathcal{E}_k - \mathcal{E}_r$, where $\mathcal{E}_r$ is the resting membrane potential. This equally applies for other ions. The equation 1.2 for overall current consists of potassium ion, sodium ion, leakage ion currents and current from membrane capacitance. The membrane is modeled as capacitor and ion channels as resistors [12]. Figure 1.2 shows the corresponding electrical circuit.

$$I = C_m \frac{\mathrm{d}V_m}{\mathrm{d}t} + g_K(V_m - V_K) + g_{Na}(V_m - V_{Na}) + g_{leak}(V_m - V_{leak}) \tag{1.2}$$

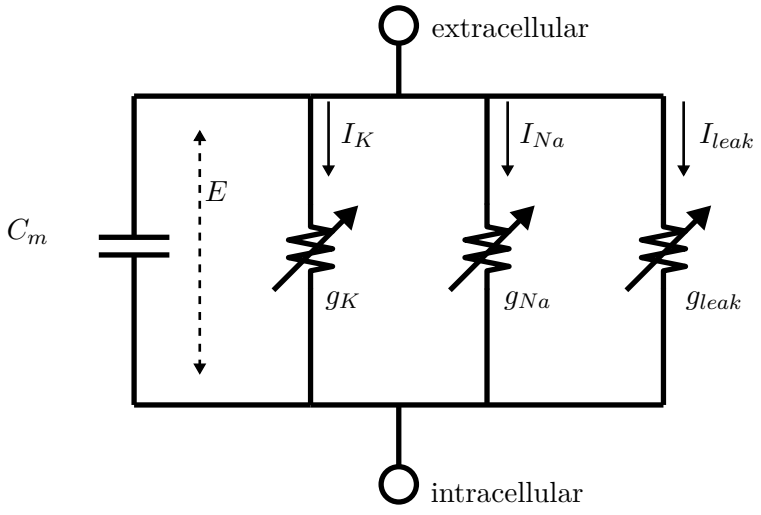

Figure 1.2: Schematic of Hodgkin-Huxley model expressed as a circuit. Figure adopted from [12].

For this equation to work the conductances must depend on time and voltage $g_i = f_i(t, V_m)$. In the Hodgkin-Huxley model the parameters h, m, n are given by first order linear differential equations. The behavior of potassium channels is described by equations 1.3 and 1.4. In their work Hodgkin and Huxley said that *"there is a little hope for calculating the time course of sodium and potassium conductances from first principles"* and so they set up a simple model for both ion channels. This is due to the limited laboratory equipment for measuring the microscopic world at that time. They made an assumption that g_K is proportional to the fourth power of a variable n which obeys first order differential equation. They thought ions were able to cross the membrane only if four similar particles occupy a specific region of the membrane. The variable n represents a portion of particles on one side of the membrane and $(1 - n)$ represents a portion of particles on the other side of the membrane. Coefficients α_n and β_n then refer to the rate of transfer of ions in and out.

$$g_K = \overline{g}_K n^4 (V - V_K) \tag{1.3}$$

$$\frac{\mathrm{d}n}{\mathrm{d}t} = \alpha_n (1 - n) + \beta_n n \tag{1.4}$$

For the sodium channel there are three equations 1.5-1.7 which describe the behavior of the channel. The sodium conductance is proportional to a number of regions of the membrane occupied by three activating molecules and not occupied by one inactivating molecule. The variable m is a portion of activating molecules and the variable h of inactivating molecules on the inside of the membrane. All three parameters m, n and h are dimensionless quantities in the interval $\langle 0, 1 \rangle$.

$$g_{Na} = \overline{g}_{Na} m^3 h (V - V_K) \tag{1.5}$$

$$\frac{\mathrm{d}m}{\mathrm{d}t} = \alpha_m (1 - m) + \beta_m m \tag{1.6}$$

$$\frac{\mathrm{d}h}{\mathrm{d}t} = \alpha_h (1 - h) + \beta_h h \tag{1.7}$$

There is no equation for the leakage conductance because it is modeled as a constant during the action potential, therefore $g_{leak} = \overline{g}_{leak}$. The parameters $\overline{g}_K$ and $\overline{g}_{Na}$ are also constants. The parameters $\alpha_h, \alpha_m, \alpha_n, \beta_h, \beta_m$ and β_n are constants which all depend on the membrane voltage V. Two equations 1.8 and 1.9 are shown for illustrating the dependency of parameters on the voltage. These equations do not have physical meaning and were obtained by purely fitting the measured data. The Hodgkin-Huxley model is invaluable for neuroscience, but it does not explain the inner workings of ion channels in much detail. The equations for conductances contain in total 12 parameters.

$$\alpha_m = \frac{0.1(V + 25)}{\exp\left(\dfrac{V + 25}{10}\right) - 1} \tag{1.8}$$

$$\beta_m = 4 \exp\left(\frac{V}{18}\right) \tag{1.9}$$

Hodgkin and Huxley distinguished two types of action potential [12]. The first type is the membrane action potential where the membrane potential is uniform across the whole lenght of the fibre. This means there is no current along the axis of the axon. The membrane current must be then zero except for the short stimulus. With the short shock at the time $t = 0$ the shape of the action potential is given by the equation 1.2 with $I = 0, V_m = V_0$ and m, n, h having their steady state values. In case of the propagating action potential the local currents have to be provided by the net membrane current as described by the equation 1.10.

$$I = \frac{l}{2R_a} \frac{\mathrm{d}^2 V}{\mathrm{d}x^2} \tag{1.10}$$

Inserting the equation 1.10 into the equation 1.2 for overall membrane current leads to a cable equation [13]. This equation is used to compute the propagating action potential.

$$\frac{l}{2R_a} \frac{\mathrm{d}^2 V}{\mathrm{d}x^2} = C_m \frac{\mathrm{d}V_m}{\mathrm{d}t} + g_K(V_m - V_K) + g_{Na}(V_m - V_{Na}) + g_{leak}(V_m - V_{leak}) \tag{1.11}$$

1.5 Other models

If one wants to simulate nerve impulses, there are many models to choose from. It is possible to select a model from the Integrate-and-fire family. Another option is to use a simplified version of the Hodgkin-Huxley model. A notable model in this category is the FitzHung-Nagumo model which consists of two nonlinear first order differential equations [14].

The problem is that these models are all purely electrical and do not explain the mechanical, thermal or optical features happening during the nerve impulse. From the mechanical point of view, it is worth mentioning the changes in the axon diameter, intracellular pressure, temperature, surface area and thickness of the membrane. Current theories which work with mechanical aspects of a nerve impulse have a weakness that while explaining certain featurers, they miss to explain the others. There exist two main categories of alternative models to the Hodking-Huxley model. One group describes the action potential as a density pulse traveling near a transition state, the other group is trying to change the originial Hodgkin-Huxley conductance model by adding mechanical features [1].

The idea that a pressure wave as a mechanical impulse underlies the propagation of information in nerves is actually older than the conductance model [15]. El Hady & Machta, 2015 formulated a numerical model in which the co-propagating mechanical displacements emerge from the surface waves due to the varying compressive electrostatic forces across the membrane [16]. Heimburg & Jackson, 2005 derived a thermodynamic theory of nerve pulse propagation in which the action potential is a localized density pulse very much resembling sound waves [17]. This model is called the soliton model. It was further proved the pulses that emerge from the model show quantitative and qualitative similarities to the action potential [18]. On the other hand, Engelbrecht et al., 2018 proposed a model where the action potential is modeled as an electrical pulse that triggers all other processes. This model is based on FitzHugh-Nagumo model that is coupled to the longitudinal and transverse mechanical waves, as well as the pressure wave in the axoplasm [19].

Chapter 2

Measuring the nerve impulse

2.1 Techniques for measuring ion currents

The recording of membrane potential can be extracellular or intracellular. The extracellular recording is suited for detecting action potentials of one or more cells. An action potential is produced by ion currents flowing in and out of extracellular space around the neuron. These currents are registered by a microelectrode. The advantage of this method is not having to perfuse the cell by microelectrode. On the other hand if the cell does not generate action potential, the microelectrode is unable to measure anything. This means that extracellular recording is used to detect whether the action potential has occurred. It is therefore used in studying neural circuits where one is not interested in the shape of the action potential [20].

The intracellular recordings require penetrating the cell. The cell cannot be used repeatedly, but this type of recordings gives more information about the action potential. The voltage clamp and the current clamp were the earliest techniques for recording ion currents. Today the patch clamp technique is frequently used which is an updated version of voltage clamp technique. Both intracellular and extracellular techniques are particularly suited for measuring excitable cells like neurons [21].

Current clamp In a current clamp setup the current is injected into the cell by a microelectrode and the voltage is free to vary. The current can be either constant or time-varying. The electrical circuit consists of a microelectrode and a buffer amplifier. The amplifier increases the current behind the signal and decreases the resistance over which the current passes. The injected current can be used to depolarize or hyperpolarize the cell and to generate action potential [21].

Voltage clamp When performing voltage clamp the voltage is controlled over a small patch. It is achieved by supplying or absorbing current to an electrical circuit. The circuit is able to hold the voltage on a given level. The current injected or absorbed is equivalent to the ionic current flowing across the membrane. The ion current arises because of the set voltage as the membrane potential is no longer the same as the resting membrane potential. The voltage clamp does not mimic a natural process but it is used rather than the current clamp. Steady voltage means the capacitance of the membrane is unchanged and there are no problems with capacitance currents. The voltage clamp is used to investigate the membrane conductance. The conductance is proportional to ion currents, and this enables to observe the opening and closing of ion channels [22].

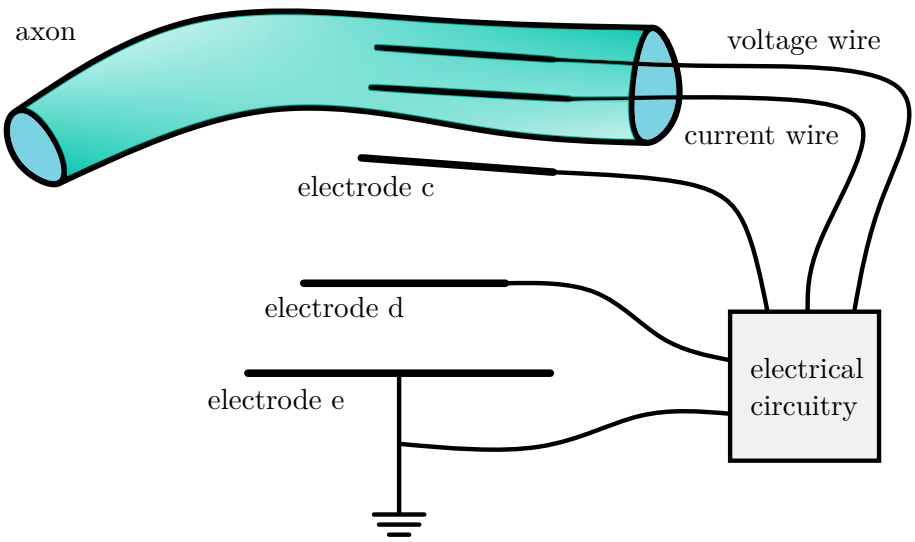

Figure 2.1: Scheme of measuring the membrane potential using voltage clamp.

Patch clamp The patch clamp technique represents a special case of a voltage clamp. It is customized for measuring currents flowing through one or few ion channels. It is equally suitable for small cells which are hard to penetrate with electrodes. The pipette for patch clamp has a narrow tip with a surface that is not sharp. The micropipette is pressed on the cell's surface, and the inner part is depressurized in order to pull the membrane to the tip. The current recorded is then ion current from very few ion channels [21].

2.2 Measurement of Hodgkin and Huxley

Hodgkin and Huxley used voltage clamp for measuring ion currents of the giant axon from the stellar nerve of Loligo forbesi. The axons have a diameter of $400-800\mu$m. Thanks to the size of axon Hodgkin and Huxley were able to perforate the axon with electrodes. One electrode recorded the action potential. The feedback amplifier then regulated the current entering the second electrode. The current was regulated to change the membrane potential quickly and hold it at a certain level. The swift change of voltage led to minimal capacitance current and enabled the study of conductance currents. For steady voltage the equation 1.2 takes the form of equation 2.1. The potassium and sodium currents were distinguished by monitoring the change of concentration of sodium ions in the extracellular space. The figure 2.1 shows a simplified version of the measurement of membrane potential by Hodgkin and Huxley in 1952 [7].

$$I = g_K(V_m - V_K) + g_{Na}(V_m - V_{Na}) + g_{leak}(V_m - V_{leak}) \tag{2.1}$$

Figure 2.2 show the data of potassium and sodium channels acquired by Hodgkin and Huxley [12]. The figure also shows the curves plotted according to the Hodgkin-Huxley model. Digitalized form of the original data is taken from [23]. The curves for each voltage were computed with the equations by which Hodgkin and Huxley fitted the data in their original text. The voltage clamp technique proved to be an enormous success because it enabled to examine only a part of the action potential. Even though the cell does not

hold a steady voltage in real impulse, these experiments helped to understand how the ion channels react to a change in membrane potential. Introducing these equations in the equation for membrane currents resulted in a fine prediction of action potential.

2.3 Measurements of mechanics and thermodynamics

Table 2.1 shows main mechanical and thermodynamical phenomena occurring during the nerve impulse. This work focuses on mechanics and therefore the changes of optical aspects are not discussed. It should be noted that these measurements were performed on nonmyelinated axons. For all measurements the action potential was invoked by outer electrical stimulus with electrodes.

During the action potential the axon is swelling. The volume and length of the axon change. The axon shortens or elongates based on the initial tension of axon. For example the Loligo giant axon elongates for positive change in volume and small tension. But if the tension is high, the axon shortens [24]. Pressure is increasing during depolarization and decreasing during hyperpolarization. With the change of length and volume, the diameter and membrane thickness of axon are also affected. With the change of membrane thickness, the conductance varies. In the Hodgkin-Huxley model the membrane conductance is assumed to be constant [25].

Tasaki measured how the action potential is accompanied by rapid lateral expansion and longitudinal shortening of axons. Few nerves tied together were placed in a water chamber. The rapid changes in hydrostatic pressure were measured by using a mechanoelectrical transducer. The chamber had four electrodes in it which were used for recording the action potential. The measuring device consisted of a diaphragm connected to a stylus. The stylus then acted on the mechanoelectrical transducer. The transducer was then connected to an operational amplifier. The volume expansion started almost immediately after the action potential and was measured between $1.0 - 2.6 \cdot 10^{-6}\text{mm}^3$ for the 15mm garfish olfactory nerve [26].

During the depolarization there is an amount of heat released. This however does not diffuse passively in the extracellular medium but most of it is reabsorbed back into the membrane. This cannot be explained by the Hodgkin-Huxley model. The model could describe heat production by simply assuming the dissipation of heat in resistors. But the electrical circuit is unable to describe the reabsorption of heat back into the membrane [25]. Abbott, Howard and Ritchie measured heat production and absorption during the action potential. They used nerves from Pacific Spider crab and lobster. A bundle of

Table 2.1: Table showing important nonelectric aspects of nerve impulse

Phenomenon	**Researcher**	**Description**
Cell swelling	Iwasa & Tasaki [26], Terakawa [27], Iwasa & Byrne [2]	Pressure of the axon rapidly changes
Heat generation and reabsorption	Abbot, Howarth and Ritchie [28], Ritchie & Keynes [29]	Heat is at first generated and then absorbed by the cell
Changes in volume of axon	Hill [24], Heimburg et al., [30]	Length and diameter of axon Changes

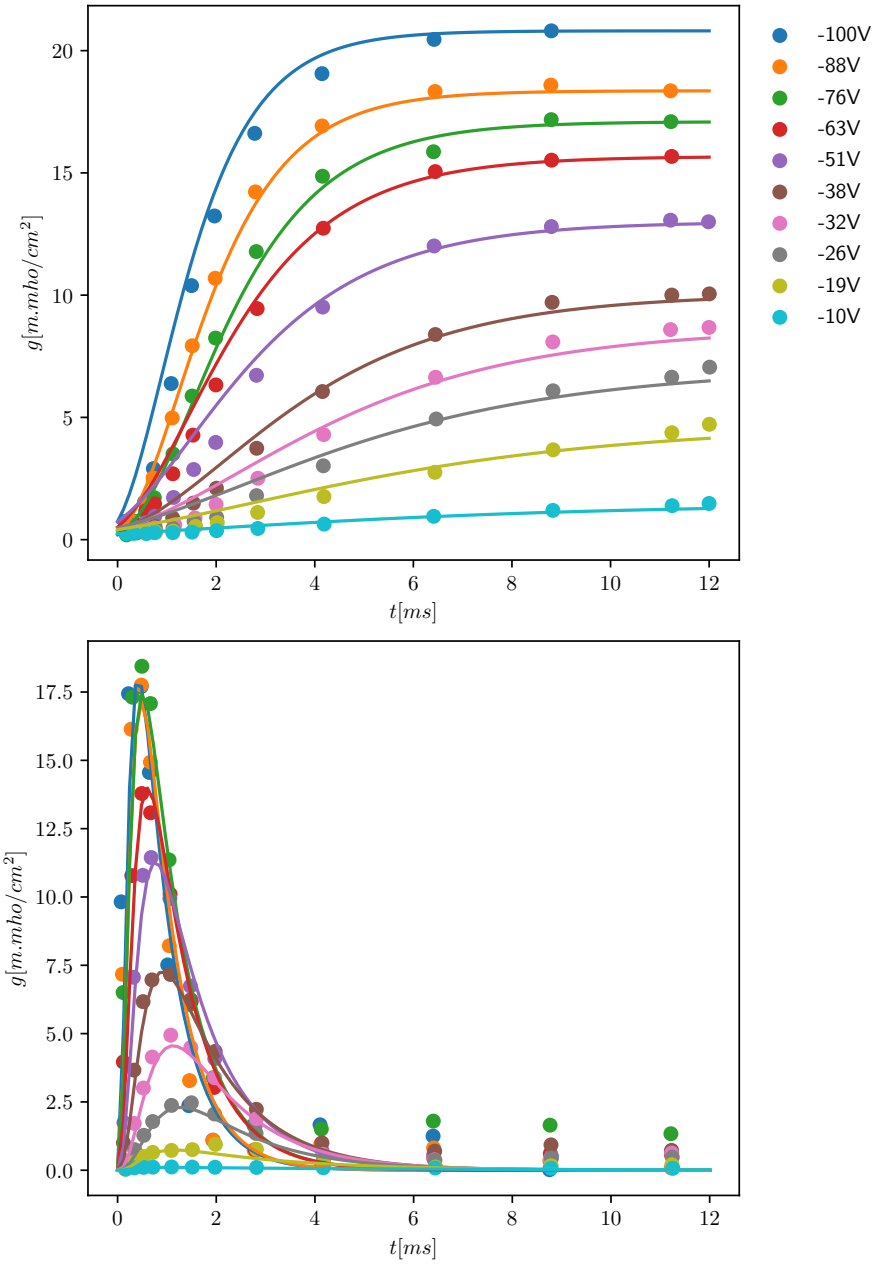

Figure 2.2: Potassium and sodium ion currents for different voltages measured on giant squid axon. The upper graph shows potassium ion current and lower graph shows sodium ion current. Data are taken from [23]. The curves are plotted with equations taken from the original text of Hodgkin and Huxley [12].

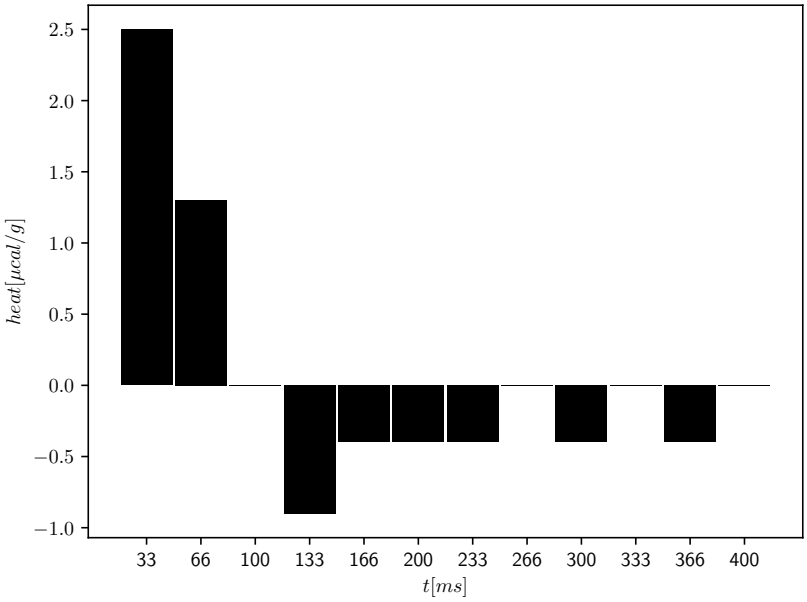

Figure 2.3: Graph of heat release and absorption during an action potential. There is a phase of heat release and a phase of heat absorption. Data adapted from [28].

nerves was mounted on a thermopile. The output from the thermopile was connected to a sensitive galvanometer and recorded. Electric shocks were applied on both ends of the bundle. The 20ms current impulse passed to the thermopile generated a heat impulse of that duration. They measured an increase in temperature of $5.2 \pm 0.6\mu$°C. After the reabsorption of heat they measured 1.0μ°C above the initial temperature [28]. The figure 2.3 shows the evolution of heat release and absorption. Because of the galvanometer and the thermophile, the recording system lagged behind the actual temperature change. Therefore, they had to analyse the data by a special method. This resulted in the fact the heat is presented in blocks with duration of 33ms.

Heimburg et al. measured the nerve thickness using the AFM technique. The nerve fibers used for this experiment were the lobster fibers. The axon was placed in a chamber with lobster saline solution. The experiment was set up to measure both mechanical impulses from AFM and electrical impulses from recording electrodes. It was discovered that the displacement of the AFM cantilever is in average about 1nm. It was also measured what happens when two impulses from the ends of the axon collide. They discovered the impulses can pass each other and they do not annihilate. [30].

Chapter 3

Goals of the thesis

Experimental results point to the fact that there occurs a number of nonelectric phenomena during the action potential. The current models do not incorporate mechanics of the excitable membrane. The main goal of this thesis is to prove that the mechanics plays an important role in describing the nerve impulse. This is performed in two ways. First a numerical model of the behaviour of ion channels is derived and second the axon diameter during the nerve impulse is studied.

The numerical model is a viscoelastic model and it is used to fit the original conductance data of Hodgkin and Huxley. This means it will be possible to describe the data by a simple mechanical model. It also means the membrane is not a passive component of the nerve impulse, but an active one. This enables to describe the behaviour of ion channels as a mechanical feature yet it would not change the structure and interpretation of Hodgkin-Huxley model. It should be, for example, easier to grasp how the viscoelastic constants vary with the change of temperature rather than to set up the dependency of temperature for the arbitrary constants in the Hodgkin Huxley model. Such a model was tried, but the result of extrapolating the fitted data to the other ones was rather unsuccessful [31].

The experimental part demonstrates the mechanical changes of axon diameter during the action potential. The cells used for the measurement are living cells which means that the action potentials occurring are spontaneous. The fact that the nerve tissue is not dead but it is capable of producing spontaneous potentials makes this experiment unique. During the experiment the axon is unaffected by any mechanical or electrical stimulus like external electrodes injecting current. These two conditions ensure not the reactions of the cell to outer causes but only the spontaneous action potential is measured. The experimental measurement showing that the action potential is directly coupled with the deformation of a cell membrane also points to the assumption that the membrane is not a passive component.

Chapter 4

Methods

4.1 General idea

A currently accepted model of the membrane is the fluid mosaic model proposed by Singer and Nicolson in 1972 [32]. It says that the membrane is a two dimensional structure made of phospholipids, proteins, carbohydrates and cholesterol. It behaves like a liquid which restricts lateral movement of intracellular components. The membrane shows both elastic and viscous (often called membrane fluidicity) properties and could be therefore modelled as viscoelastic material. A surprising fact is that mechanical stimulation of the membrane affects the behaviour of ion channels. Stretching the membrane increases the flow of ions across the membrane. This effect does not apply merely to mechanosensitive channels but also to voltage gated channels [33]. It is then reasonable to include the viscoelastic properties of the membrane in the description of the ion channels.

4.2 Numerical methods

Viscoelasticity represents a property of material which is both elastic and viscous. This means the stress is time-dependend when the material is deformed and vice versa [34]. This theory can be applied to metals at high temperatures, rubber, polymers and also to biological materials like ligaments and tendons [35]. Linear viscoelasticity is a subset of viscoelasticity. To construct a viscoelastic model, two elements are used. The first element is a spring which represents the elastic behaviour. The second element is a dashpot which represents the viscous behaviour. In linear viscoelasticity the relationship between stress and deformation (or between stress and rate of deformation for dashpot) is linear. Figure 4.1 shows the two elements and their corresponding equations. It also holds that adding two elements in parallel the deformation is the same for both elements and stress is the sum of individual stresses. For serial elements the stress is the same for both elements, and the deformation represents the sum of individual deformations. Theory of linear viscoelasticity was chosen for its simplicity. Particular class of viscoelastic materials are anelastic materials. For applied stress the material exhibits time-varying deformation. When the stress is not applied the material returns to its initial configuration. The model of a membrane for describing mechanics of ion channels was chosen to be anelastic. This means that after the end of the nerve impulse there is no residual deformation of the membrane.

A *curvefit* function from Python's optimization package Scipy was used to fit the conductance data with the ion channel model [36]. This function uses nonlinear least-squares algorithm to fit the given data to a function. The algorithm can include bounds for each

$\sigma = \eta\dot{\epsilon}$ $\sigma = E\epsilon$

Figure 4.1: Two most commonly used elements for describing viscoelastic models, a dashpot on the left and a spring on the right.

variable being fitted. The experimental data were processed in Python and filtered with the Scipy function *filtfilt*. This function applies a digital filter forward and backward to a signal. The filter itself was the fourth order lowpass Butterworth filter with the critical frequency of 25Hz.

The model consists of three parts. The first part is an assumption that the electric voltage causes the change in mechanical stress. The mechanical stress then dictates the progress of mechanical deformation which in turn affects conductance. Equations 4.1-4.3 describe a general mechanical model for an ion channel. The model assumes that the electrical voltage only affects the mechanical stress and does not influence the ion channel directly. The relationship between mechanical stress and deformation is governed by a chosen viscoelastic model. The conductance of an ion channel is affected only by the deformation in that channel and the membrane.

$$\sigma(t) = f[V(t)] \tag{4.1}$$

$$f[\sigma(t), \dot{\sigma}(t), \ldots, \sigma^{(n)}(t)] = f[\epsilon(t), \dot{\epsilon}(t), \ldots, \epsilon^{(m)}(t)] \tag{4.2}$$

$$g(t) = f[\epsilon(t)] \tag{4.3}$$

The data of potassium ion channel are similar to a solution of second order differential equation. For each value of electric voltage, the data have g_{max}. The channel's conductance steadily approaches g_{max} as can be seen from the figure 2.2. In order to fulfill this necessity, the mechanical stress should not depend directly on time but only on electric voltage. If there was any dependency on time then the mechanical stress would be a relatively complex function.

Viscoelastic models have often higher derivatives of mechanical stress and deformation. In the Hodgkin-Huxley model the electric voltage is changed from a zero value to a specific value instantly. If the mechanical stress is proportional to the electric voltage then it means the change of stress derivative is extremely large. This causes problems in the viscoelastic models. Possible solutions are either not to have higher order derivatives of mechanical stress in the equation or to have very small constants for the higher order terms.

The conductance should depend exclusively on the value of actual deformation. For example the conductance could be proportional to an area or a volume of the open channel. Both these dependencies of conductance on deformation possess simple geometrical meaning. If the conductance depends on the rate of deformation then it means the conductance is governed by the fact that the channel is being opened or closed. There is once more a problem with the potasium channel. For example a function of the form $g_{ion} = f(\epsilon)h(\dot{\epsilon})$ will be unable to describe the data. Function of the type $g_{ion} = f(\epsilon) + h(\dot{\epsilon})$ could be used but such a function has not an explicit meaning. If the conductance depends explicitly

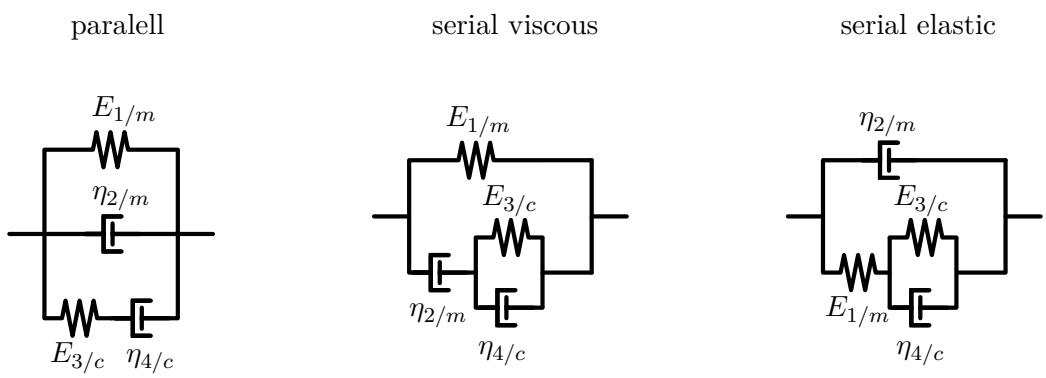

Figure 4.2: Viscoelastic models used in the overall model for an ion channels.

on time, it means that the channel proteins are being reconfigured despite of the value of deformation.

The channel could be indeed dependent on the value of electric voltage. With the electric voltage included there is not a simple way of designing a function with a clear meaning. A possible way is to say that the overall function for conductance $g_{ion} = f(\epsilon, V)$ can be separated into two independent functions $f(\epsilon)h(V)$. This means the electric voltage does not affect the deformation generated by mechanics. Throughout the thesis only the model described by equations 4.1-4.3 will be used. The viscoelastic models will consist of a maximum of four elements with derivatives no higher than the second derivative.

The viscoelastic models are constructed from two dashpots a two spring. The elements E_c, η_c represent the channel behaviour and the other elements E_m, η_m represent the membrane behaviour. Three models are derived, *serial, parallel viscous* and *parallel elastic*. If all elements are parallel the model becomes a simple Kelvin model. This model is not included because it could not describe the behaviour of ion channels. Presented models assume that both dashpot and spring should be used for a channel and membrane.

The ion channel is embedded in the membrane. When the membrane stretches because of applied stress, then the ion channel should also stretch. This implies the relationship between the channel and the membrane should be expressed in some kind of model with serial elements. This does not mean that membrane and channel elements should be strictly serial to each other. Table 4.1 shows the final equations for the chosen models. The differential equations are of second order. Right side of the equations differs only in the coefficients for the $\dot{\epsilon}$.

Parallel model It holds that $\epsilon = \epsilon_{34}$, $\sigma = \sigma_1 + \sigma_2 + \sigma_{34}$. The equation 4.4 is a constitutive equation for Maxwell model.

$$\dot{\epsilon}_{34} = \frac{\dot{\sigma}_{34}}{E_3} + \frac{\sigma_{34}}{\eta_4} \tag{4.4}$$

The $\dot{\sigma}_{34}$ and σ_{34} is then substituted by the expression for the total stress σ.

$$\begin{aligned}\dot{\epsilon} &= \frac{\dot{\sigma}_{34}}{E_3} + \frac{\sigma_{34}}{\eta_4} \\ &= \frac{\dot{\sigma} - \dot{\sigma}_1 - \dot{\sigma}_2}{E_3} + \frac{\sigma - \sigma_1 - \sigma_2}{\eta_4} \\ &= \frac{\dot{\sigma}}{E_3} - \frac{E_1}{E_3}\dot{\epsilon} - \frac{\eta_2}{E_3}\ddot{\epsilon} + \frac{1}{\eta_4}\sigma - \frac{E_1}{\eta_4}\epsilon - \frac{\eta_2}{\eta_4}\dot{\epsilon}\end{aligned} \tag{4.5}$$

$$\frac{1}{\eta_2}\dot{\sigma} + \frac{E_3}{\eta_2\eta_4}\sigma = \ddot{\epsilon} + \left(\frac{E_3}{\eta_4} + \frac{E_1}{\eta_2} + \frac{E_3}{\eta_2}\right)\dot{\epsilon} + \frac{E_3E_1}{\eta_2\eta_4}\epsilon \tag{4.6}$$

Serial viscous model It holds that $\sigma = \sigma_1 + \sigma_2$, $\epsilon = \epsilon_1 = \epsilon_2 + \epsilon_{34}$. The equation 4.7 is a constitutive equation for Kelvin model.

$$\sigma_{34} = E_3\epsilon_{34} + \eta_4\dot{\epsilon}_{34} \tag{4.7}$$

The deformations ϵ_2 and ϵ_{34} are expressed as stresses. Then the time derivative of the equation is taken in order to get rid of the $\dot{\epsilon}_2$ deformation.

$$\begin{aligned}\dot{\epsilon} &= \dot{\epsilon}_2 + \dot{\epsilon}_{34} \\ &= \frac{1}{\eta_2}\sigma_2 + \frac{1}{\eta_4}\sigma_{34} - \frac{E_3}{\eta_4}\epsilon_{34} \\ &= \frac{1}{\eta_2}\sigma_2 + \frac{1}{\eta_4}\sigma_2 - \frac{E_3}{\eta_4}(\epsilon - \epsilon_2) \\ \ddot{\epsilon} &= \left(\frac{1}{\eta_2} + \frac{1}{\eta_4}\right)\dot{\sigma}_2 - \frac{E_3}{\eta_4}(\dot{\epsilon} - \dot{\epsilon}_2) \\ &= \left(\frac{1}{\eta_2} + \frac{1}{\eta_4}\right)\dot{\sigma}_2 - \frac{E_3}{\eta_4}\dot{\epsilon} + \frac{E_3}{\eta_2\eta_4}\sigma_2 \\ &= \left(\frac{1}{\eta_2} + \frac{1}{\eta_4}\right)(\dot{\sigma} - \dot{\sigma_1}) - \frac{E_3}{\eta_4}\dot{\epsilon} + \frac{E_3}{\eta_2\eta_4}(\sigma - \sigma_1) \\ &= \left(\frac{1}{\eta_2} + \frac{1}{\eta_4}\right)\dot{\sigma} - \left(\frac{E_1}{\eta_2} + \frac{E_1}{\eta_4}\right)\dot{\epsilon} - \frac{E_3}{\eta_4}\dot{\epsilon} + \frac{E_3}{\eta_2\eta_4}\sigma - \frac{E_3E_1}{\eta_2\eta_4}\epsilon\end{aligned} \tag{4.8}$$

$$\left(\frac{1}{\eta_2} + \frac{1}{\eta_4}\right)\dot{\sigma} + \frac{E_3}{\eta_2\eta_4}\sigma = \ddot{\epsilon} + \left(\frac{E_1}{\eta_2} + \frac{E_1}{\eta_4} + \frac{E_3}{\eta_4}\right)\dot{\epsilon} + \frac{E_3E_1}{\eta_2\eta_4}\epsilon \tag{4.9}$$

Serial elastic It holds that $\epsilon = \epsilon_2$, $\sigma = \sigma_2 + \sigma_1 + \sigma_{34}$. The equation 4.10 is a constitutive equation for Kelvin model.

$$\sigma_{34} = E_3\epsilon_{34} + \eta_4\dot{\epsilon}_{34} \tag{4.10}$$

The deformations ϵ_1 and ϵ_{34} are again expressed as stresses. There is no need to take time derivative of the equation as there is no parallel viscous element to the Kelvin model.

Table 4.1: Table showing equations of the viscoelastic models

Model	**Equation**
Parallel	$\frac{1}{\eta_m}\dot{\sigma} + \frac{E_c}{\eta_m\eta_c}\sigma = \ddot{\epsilon} + \left(\frac{E_c}{\eta_c} + \frac{E_m}{\eta_m} + \frac{E_c}{\eta_m}\right)\dot{\epsilon} + \frac{E_cE_m}{\eta_c\eta_m}\epsilon$
Serial viscous	$\left(\frac{1}{\eta_m} + \frac{1}{\eta_c}\right)\dot{\sigma} + \frac{E_c}{\eta_m\eta_c}\sigma = \ddot{\epsilon} + \left(\frac{E_m}{\eta_m} + \frac{E_m}{\eta_c} + \frac{E_c}{\eta_c}\right)\dot{\epsilon} + \frac{E_cE_m}{\eta_c\eta_m}\epsilon$
Serial elastic	$\frac{1}{\eta_m}\dot{\sigma} + \frac{E_m + E_c}{\eta_m\eta_c}\sigma = \ddot{\epsilon} + \left(\frac{E_c}{\eta_c} + \frac{E_m}{\eta_c} + \frac{E_m}{\eta_m}\right)\dot{\epsilon} + \frac{E_cE_m}{\eta_c\eta_m}\epsilon$

$$
\begin{aligned}
\dot{\epsilon} &= \dot{\epsilon}_1 + \dot{\epsilon}_{34} \\
&= \frac{1}{E_1}\dot{\sigma}_1 + \frac{1}{\eta_4}\sigma_{34} - \frac{E_3}{\eta_4}\epsilon_{34} \\
&= \frac{1}{E_1}(\dot{\sigma} - \dot{\sigma}_2) + \frac{1}{\eta_4}\sigma_1 - \frac{E_3}{\eta_4}(\epsilon - \epsilon_1) \\
&= \frac{1}{E_1}\dot{\sigma} - \frac{1}{E_1}\dot{\sigma}_2 + \frac{1}{\eta_4}(\sigma - \sigma_2) - \frac{E_3}{\eta_4}\epsilon + \frac{E_3}{E_1\eta_4}(\sigma - \sigma_2) \\
&= \frac{1}{E_1}\dot{\sigma} - \frac{\eta_2}{E_1}\ddot{\epsilon} + \frac{1}{\eta_4}\sigma - \frac{\eta_2}{\eta_4}\dot{\epsilon} - \frac{E_3}{\eta_4}\epsilon + \frac{E_3}{E_1\eta_4}\sigma - \frac{E_3\eta_2}{E_1\eta_4}\dot{\epsilon}
\end{aligned}
\tag{4.11}
$$

$$
\frac{1}{\eta_2}\dot{\sigma} + \frac{E_1 + E_3}{\eta_2\eta_4}\sigma = \ddot{\epsilon} + \left(\frac{E_3}{\eta_4} + \frac{E_1}{\eta_4} + \frac{E_1}{\eta_2}\right)\dot{\epsilon} + \frac{E_3E_1}{\eta_2\eta_4}\epsilon \tag{4.12}
$$

At this time it is possible to define a more concrete version of the ion channel model. It is assumed that mechanical stress is directly proportional to electric voltage $\sigma(t) = aV(t)$. The conductance is proportional to a third power of deformation $g = b\epsilon^3$. The equations 4.13-4.15 are the final equations used for fitting the conductance data of ion channels.

$$
\sigma(t) = aV(t) \tag{4.13}
$$

$$
f[\sigma(t), \dot{\sigma}(t)] = f[\epsilon(t), \dot{\epsilon}(t), \ddot{\epsilon}(t)] \tag{4.14}
$$

$$
g(t) = b\epsilon^3(t) \tag{4.15}
$$

To perform an optimization process the solution to the differential viscoelastic equation is needed. The solution was found numerically. It is possible to obtain an analytical solution to a second order differential equation but the optimization algorithm was essentially performing better using the numerical solution. A seventh order Runge-Kutta explicit method was used to solve the viscoelastic equation. In the Scipy package it is the DOP853 routine. The explicit methods are typically used for non-stiff equations. The problem is to recognize whether the equation is stiff [37]. A care must be taken as the sodium channel contains a sharp peak where the solution can experience problems. To compare the ability of DOP853 routine to solve the equation an implicit Runge-Kutta method of Radau family was used. The corresponding routine of the implicit method is called Radau. An equation with similar shape of solution to sodium curves was solved analytically. Both routines were tested by solving the equation with a known solution.

Both were capable of solving the equation with the explicit routine needing less steps. Therefore the routine DOP853 was used for both channels.

4.3 Experimental methods

The AFM is one type of the scanning probe microscopes. It is widely used to study biological samples because there is no need for coating or staining. The samples can be imaged in physiological conditions [38]. Although it is called a microscope, it is very different from optical microscopes. AFM gathers data in the form of displacement and force measurements which are then processed in a computer. Of course there is a lens, a light source and an eyepiece integrated for viewing the sample as one would find in a normal microscope, but these components are not used in the process of data gathering.

The principle of AFM is highly mechanical. The system consists of a cantilever with a probe attached to it, a laser emitting device and a photodiode. A laser beam is deflected from the cantilever, and this is registered by the photodiode. As the probe makes contact with a sample, the sample exerts a force on the probe which in turn causes the cantilever to bent. The bent cantilever deflects the laser beam differently and this change is captured by the photodiode. If the spring constant of the beam and the change of deflection are known, it is possible to compute the force exerted by the sample on the probe [39]. Figure 4.4 shows the schematics of the AFM.

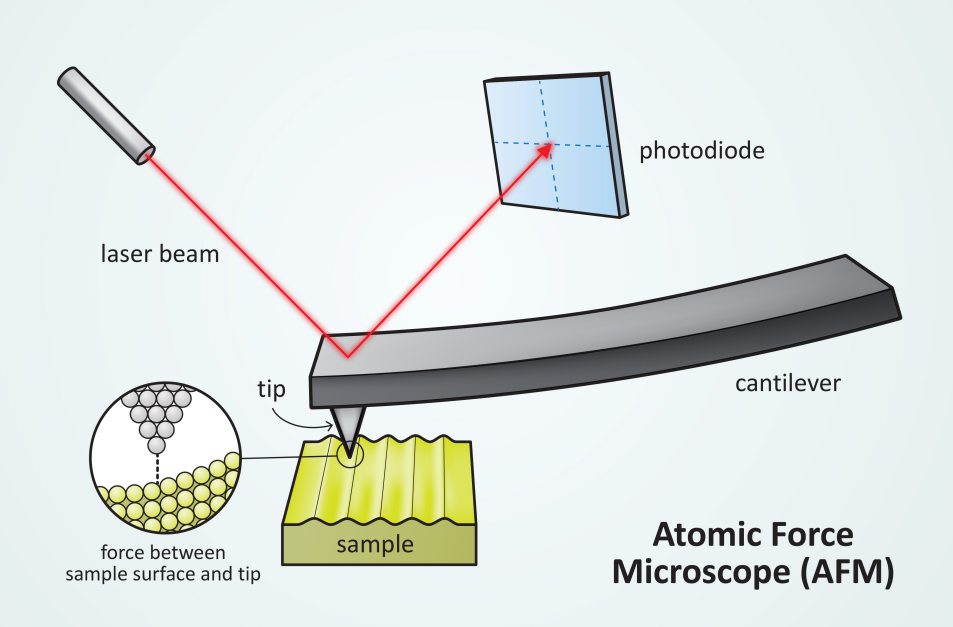

Figure 4.3: Schematics of Atomic force microscope. Figure adopted from [40].

The AFM is able to work in various modes [39]. The data in this work were obtained with the *constant force* mode. In this mode the AFM is set up to keep constant force in the sample-cantilever interaction. This is accomplished by using feedback loop which monitors the cantilever response. If the force on the sample is too big, the cantilever is elevated to maintain the set force. Similarly, if the force is too low, the cantilever is lowered. This is better than keeping the cantilever in a fixed position because the probe will not exert a force big enough to damage the sample [38].

The AFM records following data, *time, height, vertical deflection* and *horizontal deflection*. From these four types of information, only the time and vertical deflection records are used. The height is the overall result of the position of the cantilever and it experiences temperature shift. The protocol describes the calibration of the spring constant which is the vertical rigidity of the cantilever. The torsional rigidity of the cantilever was not calibrated, therefore, the data of horizontal deflection are of no concern.

The vertical deflection is the actual thing which is being measured. With the calibrated spring constant, the vertical deflection is converted to a force. The data presented here are therefore described as *force* data. Another measured quantity is the height data. In order to keep the force steady the height of the cantilever must be changing. This is achieved by moving the base of the cantilever by piezoelectric component. The height of the base is measured independently of the force measurement and is described as *height* data.

The methodology of measuring the cells is summarized in an attached protocol, see appendix A. The cells were prepared at the Institute of Experimental Medicine, Czech Academy of Sciences. The cells needed to be transported to the Faculty of Biomedical Engineering, Czech Technical university in Prague. The faculty of Biomedical engineering features an incubator capable of sustaining prescribed temperature and atmosphere. During the transport the cells were kept in a storage box with controlled temperature. The transport itself could affect the health of the cells. The cells could not be cultivated right at the Faculty as at that time the laboratory was not arranged for such tasks. After arrival the cells were transferred to the incubator and left there for 1-2 hours. The AFM needs to be set up for the actual measurement. This consists primarily of calibrating the cantilever, and it is also described in the protocol.

After recovering in the incubator, the cells were placed in the AFM. The AFM does not feature temperature or atmosphere control. This means the cells begin to die. It was decided to perform 2-3 20 minute measurements on a single cell population and then declare the cells as incapable of firing action potentials. Figure 4.4 contains four screenshots presenting the degradation of neurons with time.

The neurons normally have one axon and few dendrites. The diameter and length vary for different animals. For example the squid giant axon is a large axon. Its diameter can be over a millimeter and it spans from the head to the top of the squid's body. This makes the axon well recognizable from other neurites. The problem is mouse cells do not have such giant axons. There are few differences between axons and dendrites. An axon should have a uniform diameter, be very long and branch at its end, contrary to a dendrite. In fact these differences tend to be very difficult to classify which means there is no easy way of selecting an axon when looking at cell's culture through a microscope. The dendrites are capable of initiating similar spikes to action potentials called dendritic spikes. The action potentials can also backpropagate to axon's body and further into the dendrites [41]. This is a problem when one wants to measure only spikes generated by axons.

4.4 Visualization of axons

One way of characterizing axons in cells under a fluorescent microscope is the use of GFP - Green fluorescent protein. Specific surface axonal proteins can be tagged with the GFP. As the proteins flow through the axons carrying the GFP, it is theoretically possible

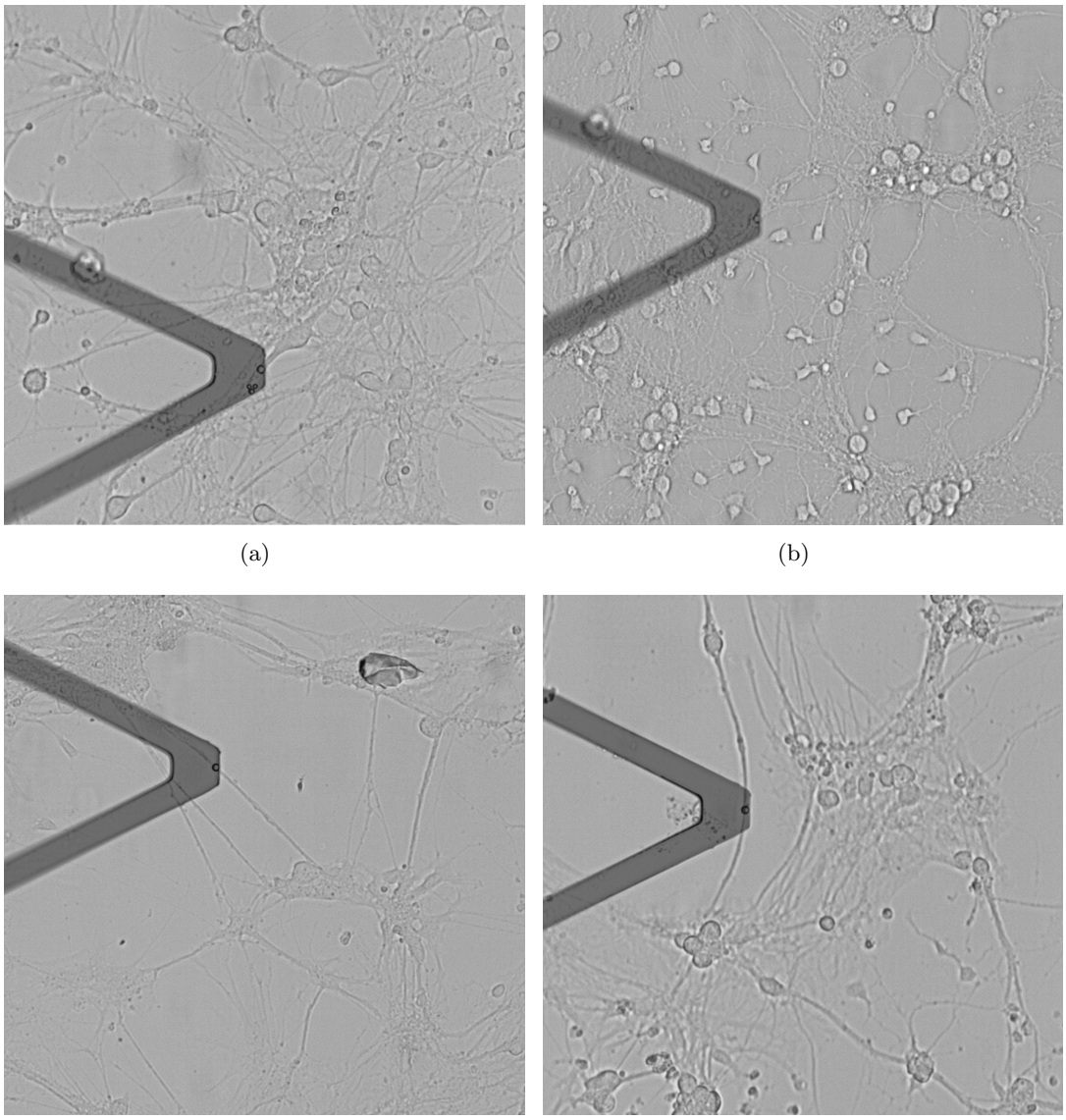

(a) (b)

(c) (d)

Figure 4.4: Pictures of cells showing degradation in time due to uncontrolled temperature and atmosphere. Picture (a) represents first measured cells, picture (b) after an hour. Picture (c) shows another living cells and picture (d) after 30 minutes.

to distinguish axons from dendrites. The AFM microscope used for the measurement did not include fluorescence optics. Instead the nanoindenter located at the Faculty of Mechanical Engineering, Czech Technical University in Prague, was used for inspecting the stained axons. This means that even after locating the axons by means of fluorescence, there is no way of transferring this information to the AFM microscope. When looking at the fluorescent axons, it was also impossible to establish any more precise criterion by which to differentiate the axons when not stained by GFP. The nanoindenter could not be used because it does not have required resolution for performing the measurement. Figure 4.5 shows photographs taken by the fluorescent microscope in nanoindenter.

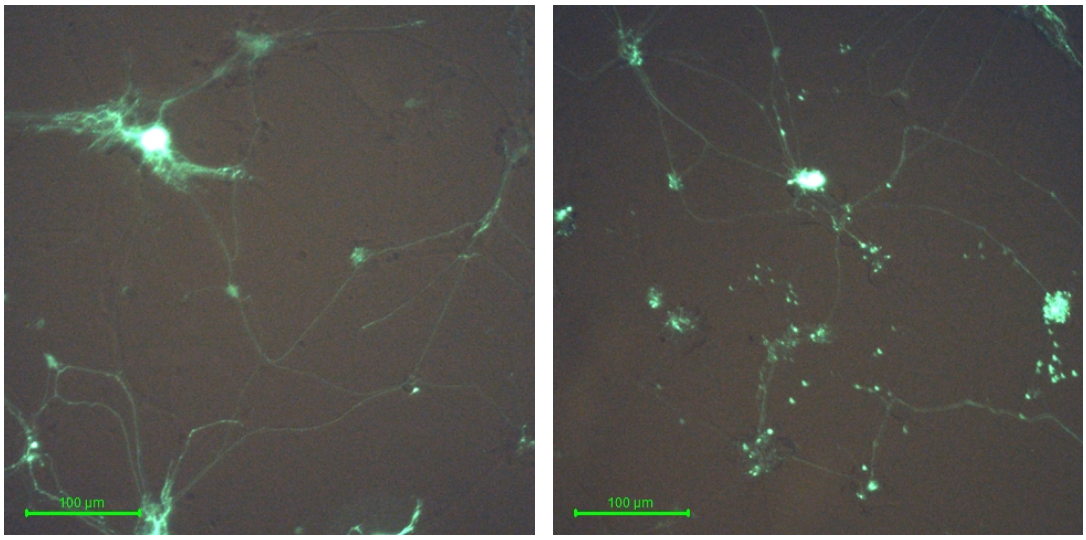

(a) (b)

Figure 4.5: Pictures of glowings cells thanks to GFP.

4.5 Criterions for data

It is not odd at all that nerve cells produce action potentials with different duration. It was found out mouse neurons are firing action potentials with duration around $25ms$ and $130ms$ [42]. The impulses which were measured by AFM have duration about $50ms$ for the fast ones and $170 - 190ms$ for the longer ones. Longer impulses were attributed to other physical phenomena. Impulses with amplitudes several magnitudes bigger were thought to be a device error. The impulse must have the response in both force and height data. Many impulses were only visible in the measurement of the force. The shape of expected mechanical impulse was said to be similar to the shape of action potential. More precisely the height measurement was expected to have some kind of coupling with the electrical phenomenon via the change of curvature during the action potential.

The action potentials of other mouse cells were measured at Czech Academy of Sciences at the Institute of Experimental Medicine. The neurons were similar to which were used for the AFM measurement. Cell types DIV 15 and 16 were measured for the electrical phenomenon and cell type DIV 17 was measured for the mechanical phenomenon. The potentials were measured using the current clamp technique with the current value of 50pA. As the value of the current is so small it can be said that the action potentials are almost spontaneous. The figure 4.6 shows selected measurements of action potentials on the neurons. The durations of measured action potentials can be divided into three groups, $15ms, 25ms$ and $30ms$. The start of the potential is the time of steepest ascend and the end is the lowest measured point.

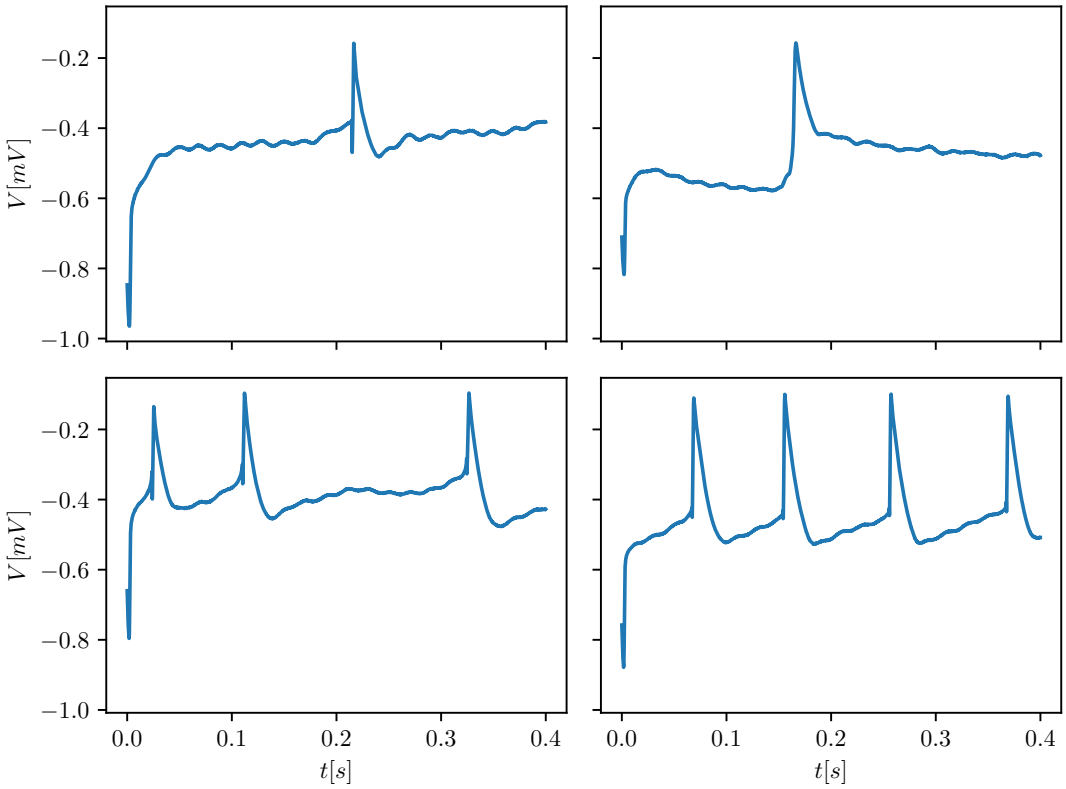

Figure 4.6: Sample data of electrical measurement of action potentials provided by the Institute of Experimental Medicine, CAS.

Chapter 5

Results

5.1 Numerical results

All six parameters of the resulting model were fitted, $E_m, E_c, \eta_c, \eta_m, a, b$. The first four parameters represent the mechanics of viscoelasticity and the other two represent a transformation from or to voltage conductance. The lower bound for potassium channels was $[0, 0, 0, 0, -50, 0]$ and the upper bound $[150, 500, 50, 500, 0, 200]$. For sodium channel the lower bounds were $[0, 0, 0, 0, 0, 390]$ and the upper bounds were $[300, 300, 500, 500, 300, 900]$. First the initial guess was left to be chosen by the algorithm. After few trials the best fit for each channel was chosen and set as initial guess. For the potassium channel the values of initial guess are $[9.500, 4.676, 9.994, 3.457, -3.803, 1.405]$ and for the sodium channels $[8.853e-03, 4.571e-09, 1.372e-03, 415.181, 0.256, 391.000]$.

Figures 5.1-5.6 show the results of the fitting process. The potassium channel can be fitted with any model. If the parameters are inspected more closely, it can be noted that the parallel model is the best option. Figure 5.1 represents the parallel model. There the membrane elasticity E_m is increasing but channel elasticity E_c and membrane viscosity η_m is decreasing with increasing depolarization. This means that for high negative voltage the membrane is more stiff but the ion channel stiffness is decreasing. The parameters η_c, a and b are constant and then vary for small voltage values. The serial elastic model shown by the figure 5.2 is similar to the parallel model for most parameters with the exception that the membrane elasticity E_m and channel elasticity E_c differ for the small voltage values. The serial model shown by the figure 5.3 has much less varying values for the channel elasticity E_c. As the previous two models, it does not handle the small voltage values well. The sodium channel can be fitted only by the parallel model. The membrane elasticity E_m is decreasing and the channel elasticity E_c is increasing with increasing depolarization. The other two models show negative conductance for the sodium channel which is not physically possible.

Apart from these parameters, the initial values $\epsilon(0)$ and $\dot{\epsilon}(0)$ need to be specified. For the potassium channels these values were set to be $\epsilon(0) = 0$ and $\dot{\epsilon}(0) = 0.7$ and for sodium channel $\epsilon(0) = 0$ and $\dot{\epsilon}(0) = 0.9$. It is reasonable to assume the initial deformation is very small. If not, then the model predicts nonzero conductance according to equation 4.15. The initial deformation was therefore set to zero. The problem is the initial rate of deformation. The values around 1.0 yield best results for the fit to both potassium and sodium channel. The potassium channel seems to be relatively independent on the initial rate of deformation. This is no longer true for the sodium channel.

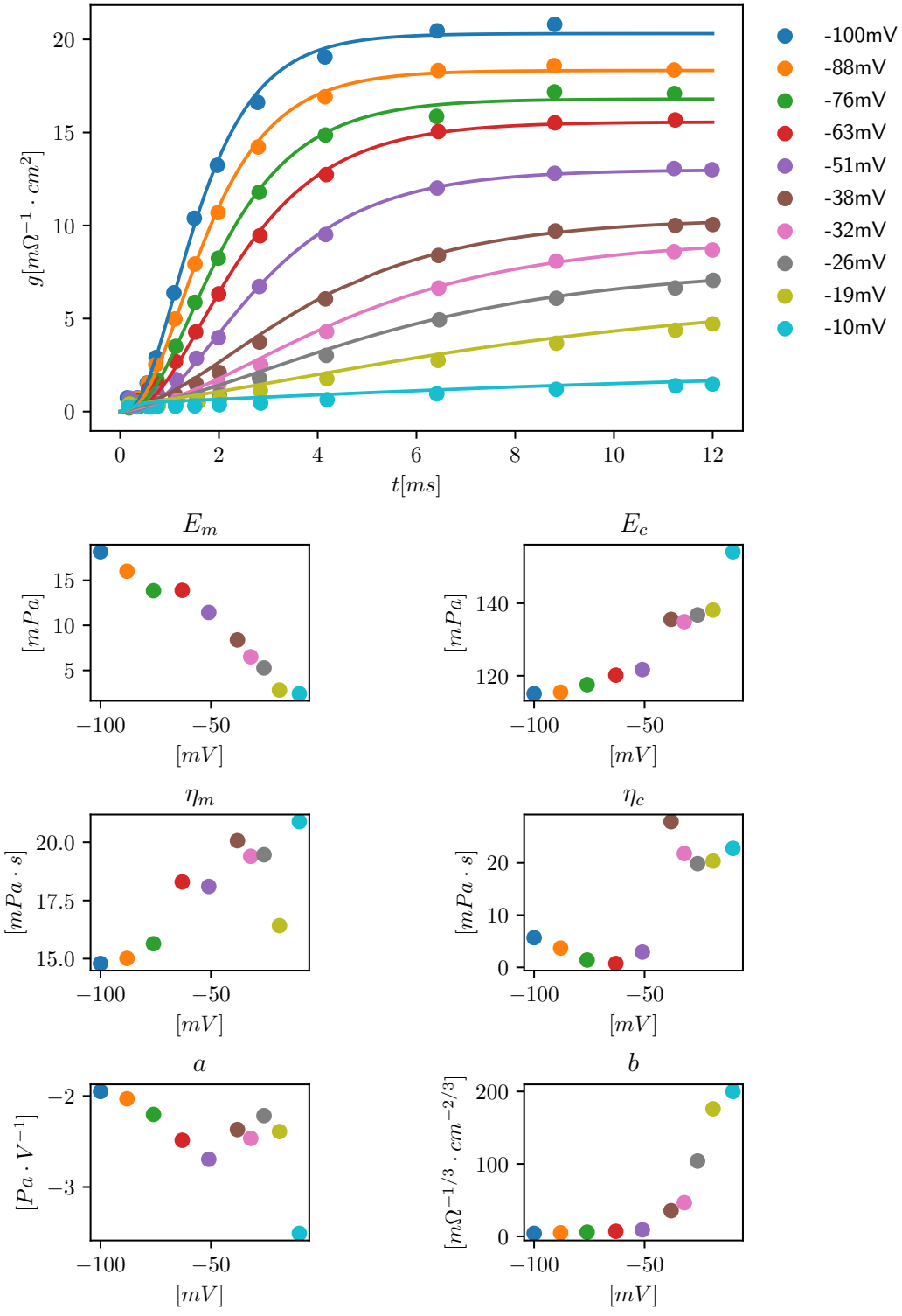

Figure 5.1: Fitting potassium channel with the parallel model.

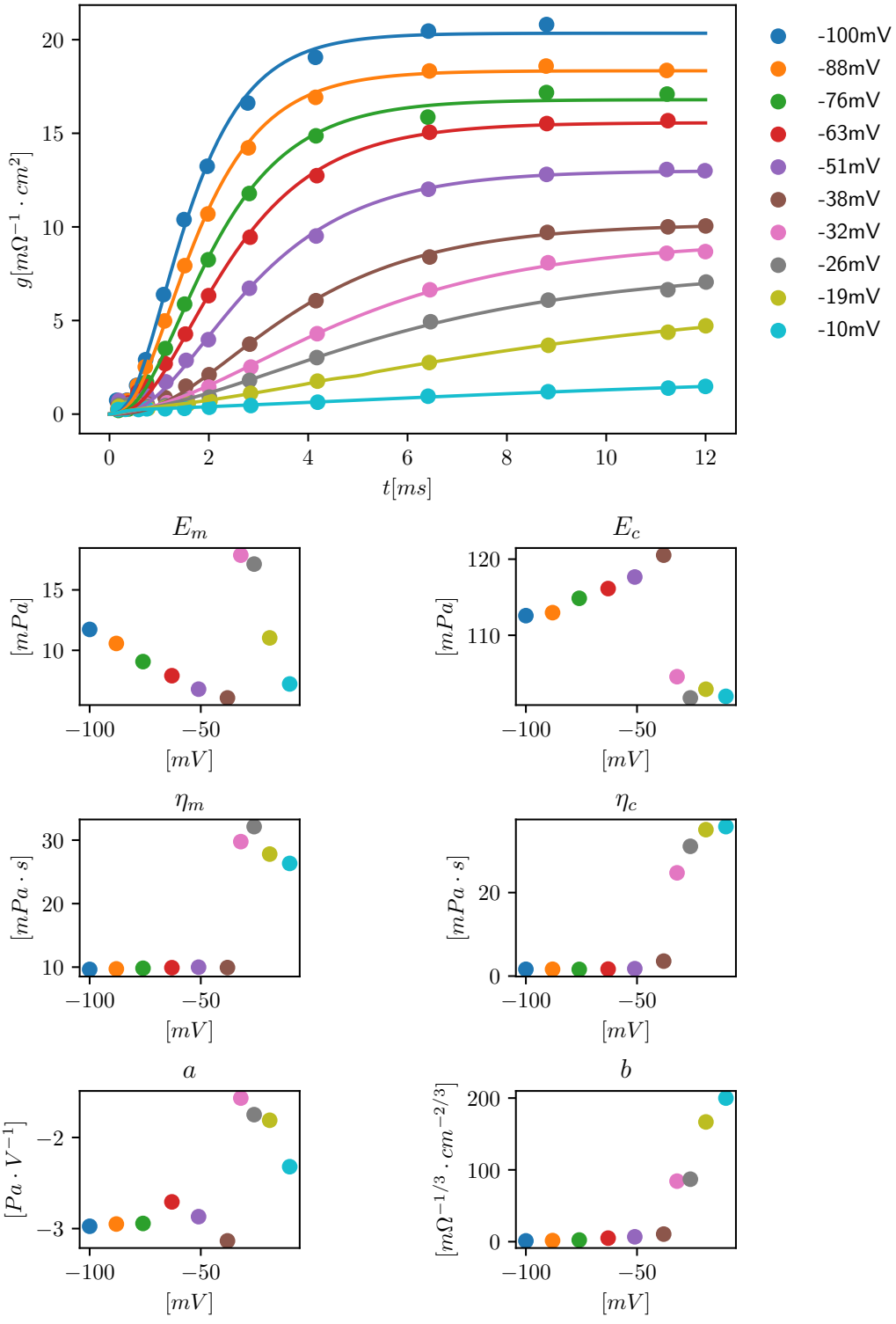

Figure 5.2: Fitting potassium channel with the serial viscous model.

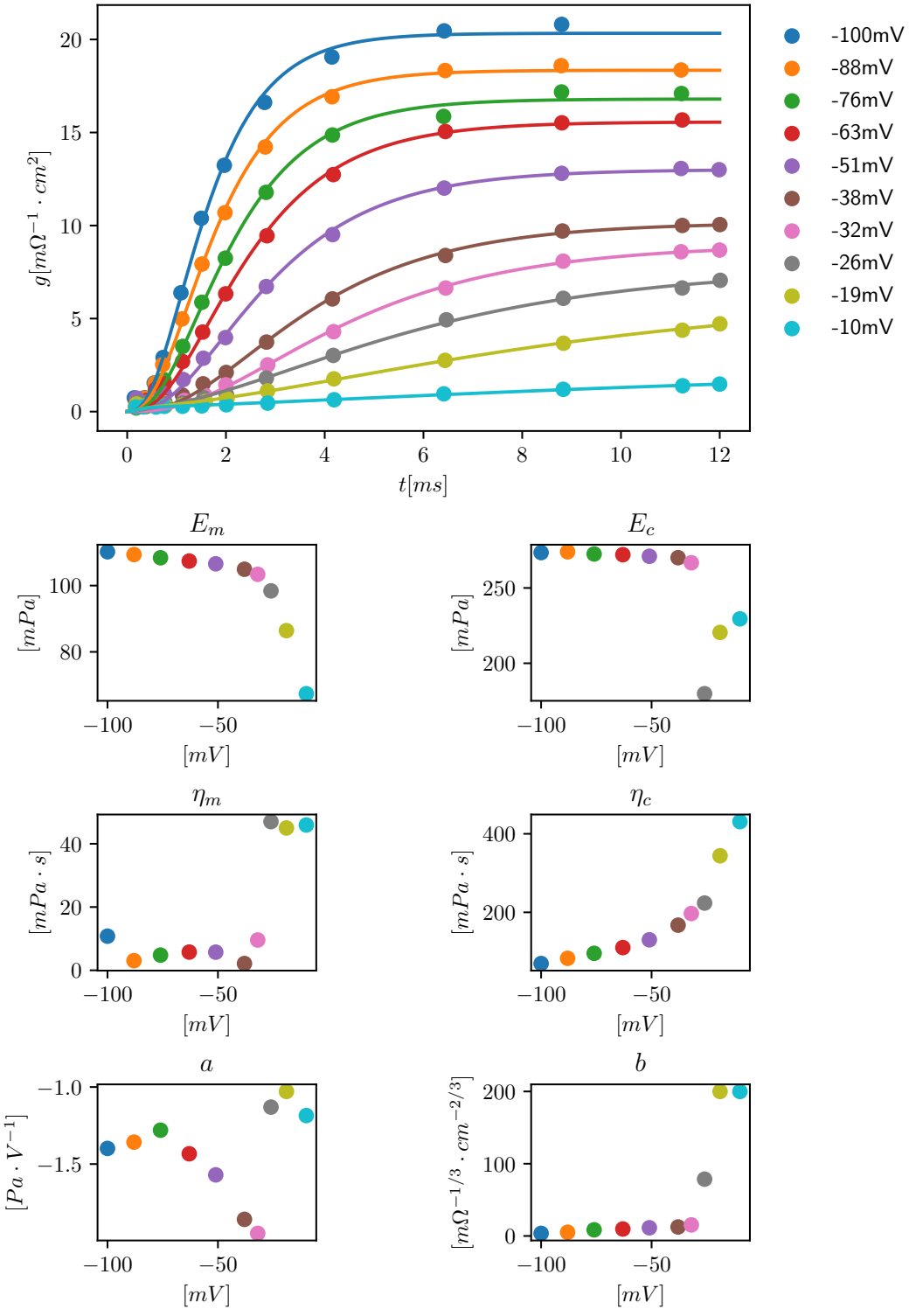

Figure 5.3: Fitting potassium channel with the serial elastic model.

Figure 5.7 shows comparison of the results from fitting. The first graph has fixed initial condition for $\dot{\epsilon}(0)$. the second graph shows what happens, when the initial value is included in the fitting process. The bounds for the initial conditions were $[0, 10]$ and initial guess was 1.0. One can ask what the deformation $\epsilon(t)$ represents specifically. The value of $\epsilon(t)$ in the equation 4.15 represents the value of deformation for the whole viscoelastic model. But this is not the only option for the deformation. For example the deformation can be defined as the deformation of the elastic element E_c as the deformation of just the ion channel. This deformation ϵ_{ch} can be computed directly by equation 5.1 where the ϵ represents the deformation of the whole viscoelastic model.

$$\epsilon_{ch} = \frac{\sigma}{E_c} - \frac{E_m \epsilon}{E_c} - \frac{\eta_m \dot{\epsilon}}{E_c} \tag{5.1}$$

Computing deformation ϵ_{ch} for serial viscous model results in solving differential equation described by equation 5.2.

$$(1 + \eta_m \eta_c)\dot{\epsilon}_{ch} + \eta_m E_c \epsilon_{ch} = \dot{\epsilon} \tag{5.2}$$

The equation 5.1 was incorporated in the parallel model in order to fit the data with the deformation ϵ_{ch}. This means the conductance would depend on the deformation of the ion channel. It was however not possible to fit the data using this model.

It is possible that the parameters a and b are voltage dependent and need to be involved in the fitting process. However the models assume that mechanical stress is proportional to the electrical voltage and the ion conductance is thought to be proportional to deformation. It is then odd to have these coefficient change with voltage. The script which fits the data was modified to keep a and b constant for all values of voltage. For this purpose the parallel model was used. It was not successful to fit the sodium channel even when the $\dot{\epsilon}(0)$ was added to the fitting process. For the potassium channel this caused quite an improvement. It was possible to express the relationship between the constants E_c, E_m and η_c and voltage with linear dependency. Figure 5.8 shows conductance data and graphs of the four parameters. The other two parameters were set to $a = -2.5$ and $b = 100$. Three of the four parameters were then taken to be linearly dependent on the voltage. This is indicated by black dashed lines. The equations for these parameters are 5.3,5.4 and 5.5. This parallel model with four variables and two constants is suitable for describing the potassium data. Both membrane and channel elasticities are increasing with increasing depolarization while the membrane viscosity is decreasing.

$$E_c = 4.487 - 0.342V \tag{5.3}$$

$$E_m = 53.909 - 3.764V \tag{5.4}$$

$$\eta_c = 51.508 + 0.161V \tag{5.5}$$

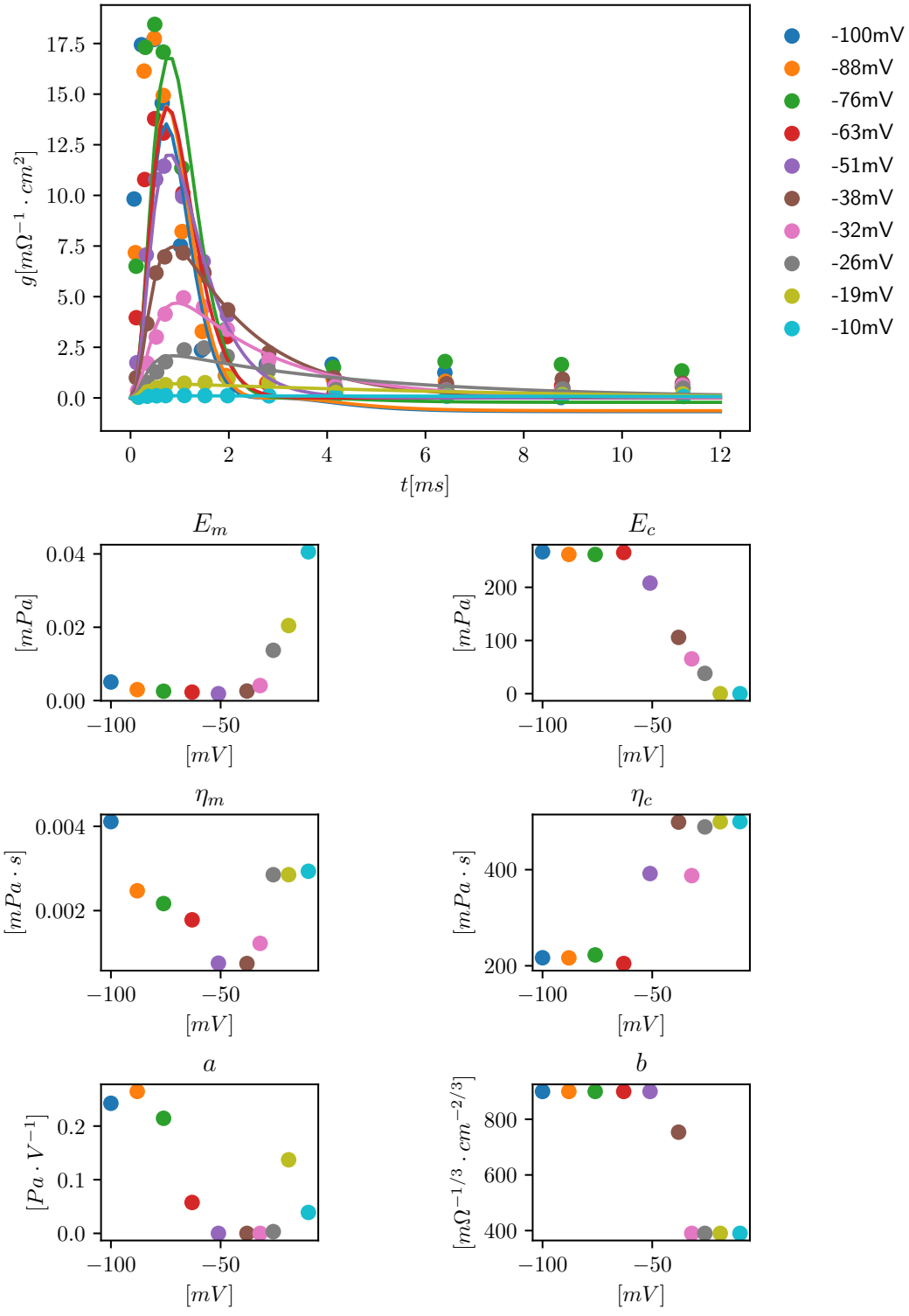

Figure 5.4: Fitting sodium channel with the parallel model.

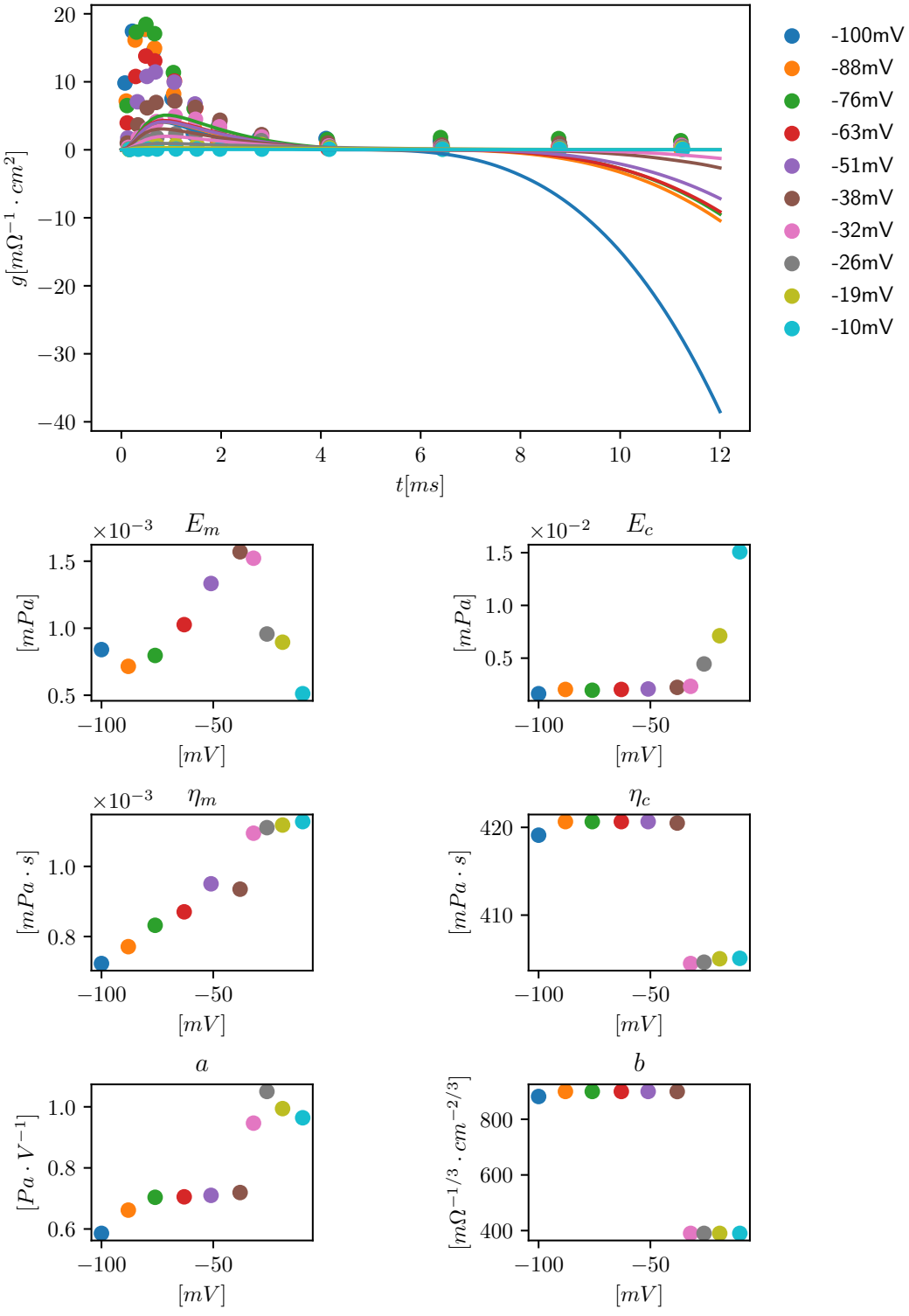

Figure 5.5: Fitting sodium channel with the serial viscous model.

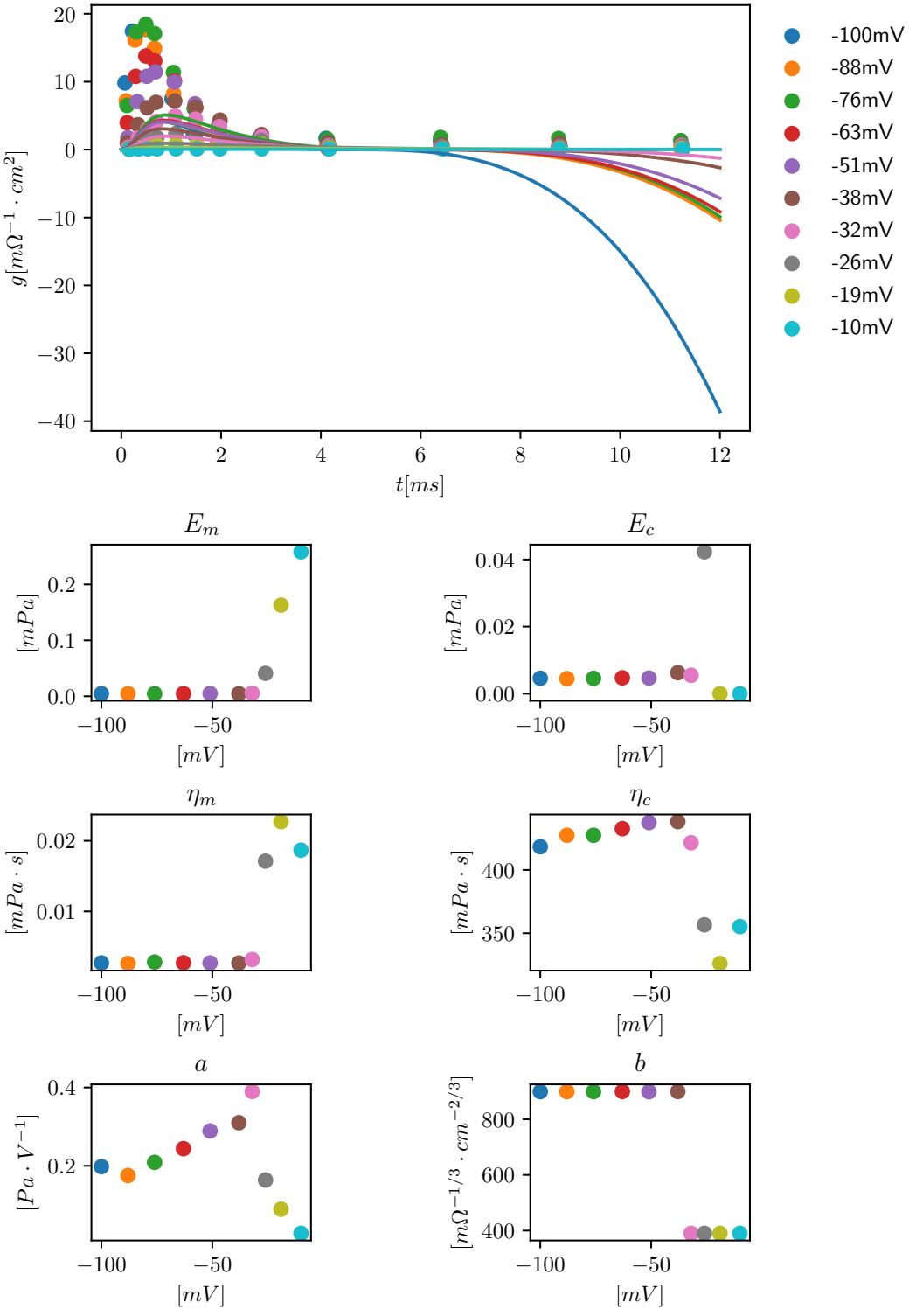

Figure 5.6: Fitting sodium channel with the serial elastic model.

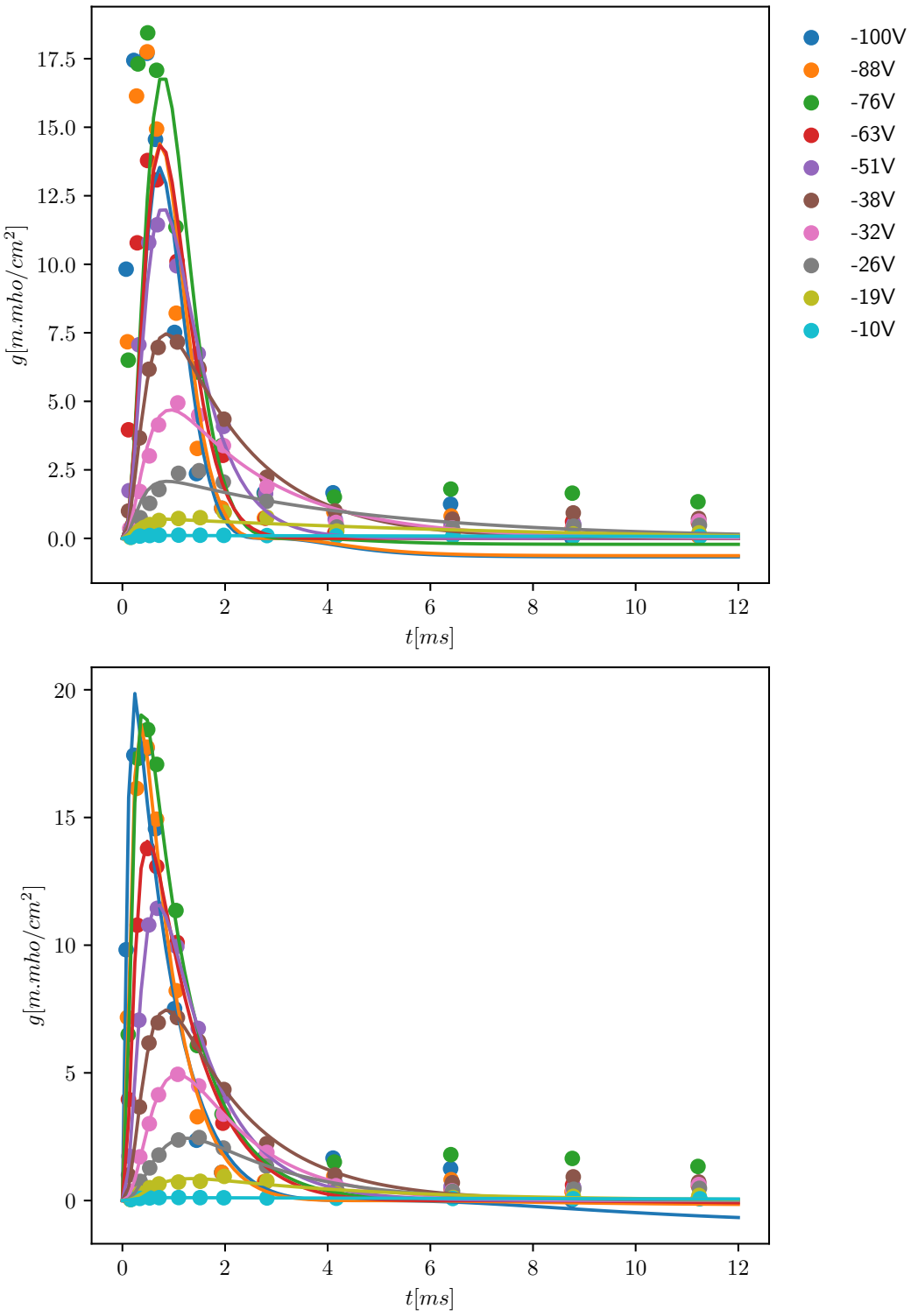

Figure 5.7: Comparison of different fits for the sodium channel. The first graph was fitted only with viscoelastic parameters. Second graph represent a result from fitting the viscoelastic parameters and also the initial condition for derivative, $\dot{\epsilon}(0)$.

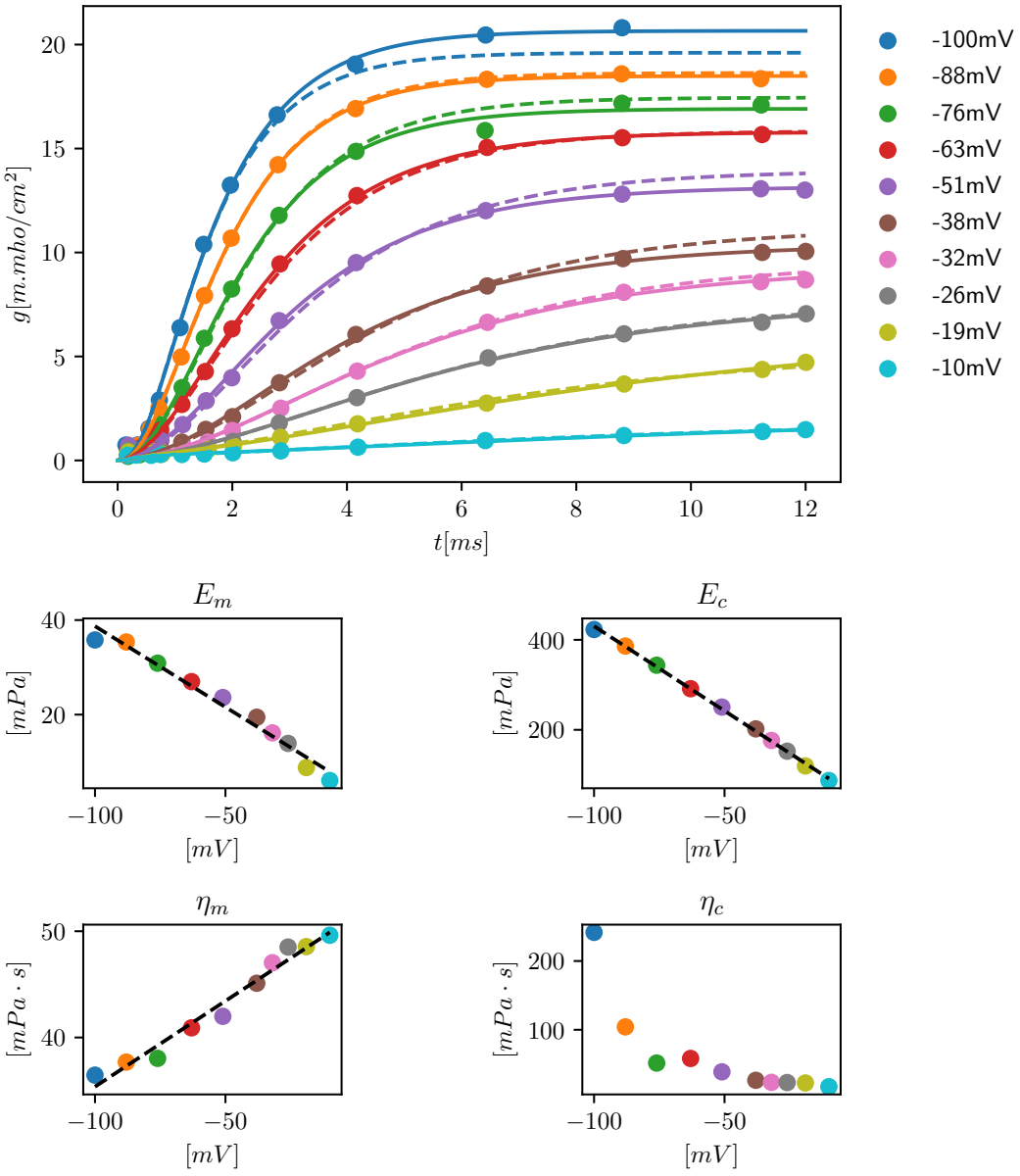

Figure 5.8: Parallel model for potassium channel with four coefficients. The upper graph shows two types of lines. The solid lines represent the curves computed with parameters from the lower graphs. The dashed lines represent the curves computed by parameters given by equations.

5.2 Experimental results

Altogether 26 samples were measured which resulted in over 60 individual 20-minutes axon measurements. Figures 5.9, 5.10 and 5.11 shows data of impulses thought to be mechanical records of neural activity. The graphs show the force and height measurements. Apart from that they also show filtered force data.

Table 5.1: Table showing the results from AFM measurement

Data	**Impulse duration in** ms	**Impulse height in** nm
data from figure 5.9	193 ± 50	9.1 ± 3.8
data from figure 5.10	168 ± 31	13.1 ± 4.0
data from figure 5.11	51 ± 12	16.9 ± 7.5

Table 5.1 shows the duration and height of the impulses from the height data. Three groups of mechanical impulses were selected from the overall data. All impulses were superposed to start simultaneously. The duration of the impulse was measured from the start of the impulse to the point, where the height was at the same level as in the beginning. The height was measured from the rest position to the maximum height of the impulse. The figure 5.9 has longest impulses, 193 ± 50ms, with low amplitudes 9.1 ± 3.8nm from all the data. The figure 5.10 has slightly shorter impulses than the first group with similar amplitude. The last figure 5.11 has shortest impulses 51 ± 12ms, but with biggest amplitudes 16.9 ± 7.5nm. This set of data has another difference, that being the less number of frequencies recorded. This can be seen from the filtered force data. The data are cleaner than the previous ones. The cantilever used was the same for all measurements. The sole difference was the tip used. The tip was, however, the identical type and package as the first one.

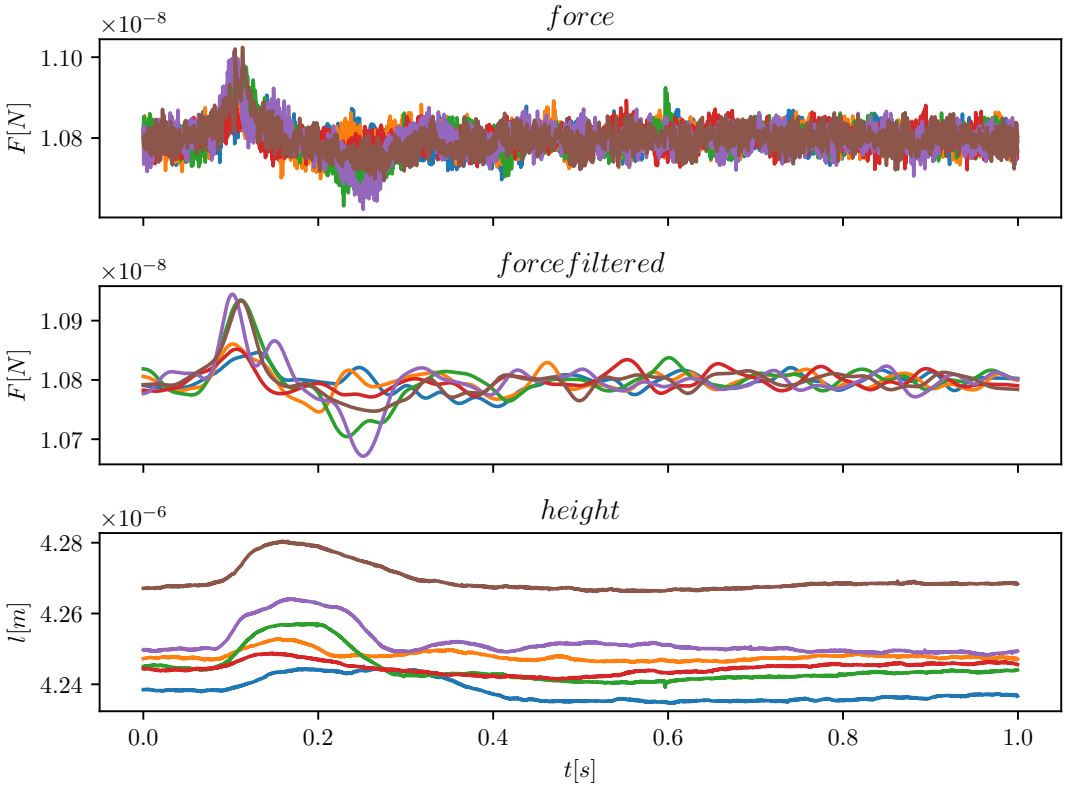

Figure 5.9: Data from AFM measurement. Six impulses shown.

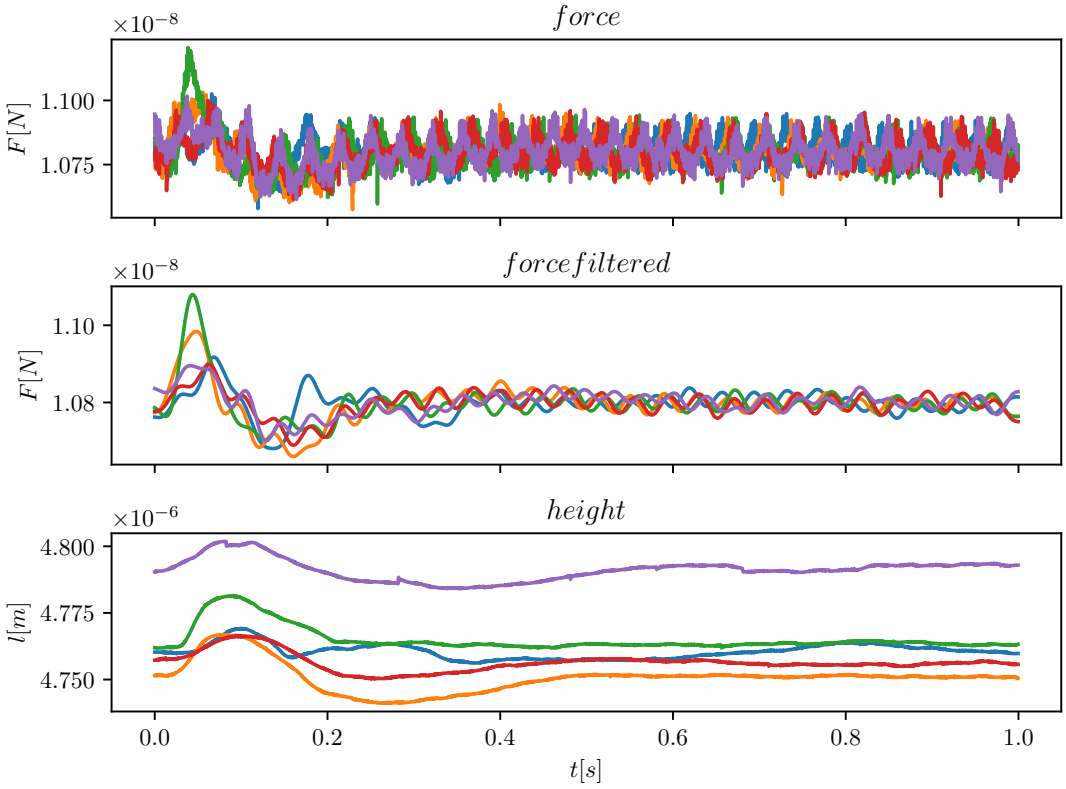

Figure 5.10: Data from AFM measurement. Five impulses shown.

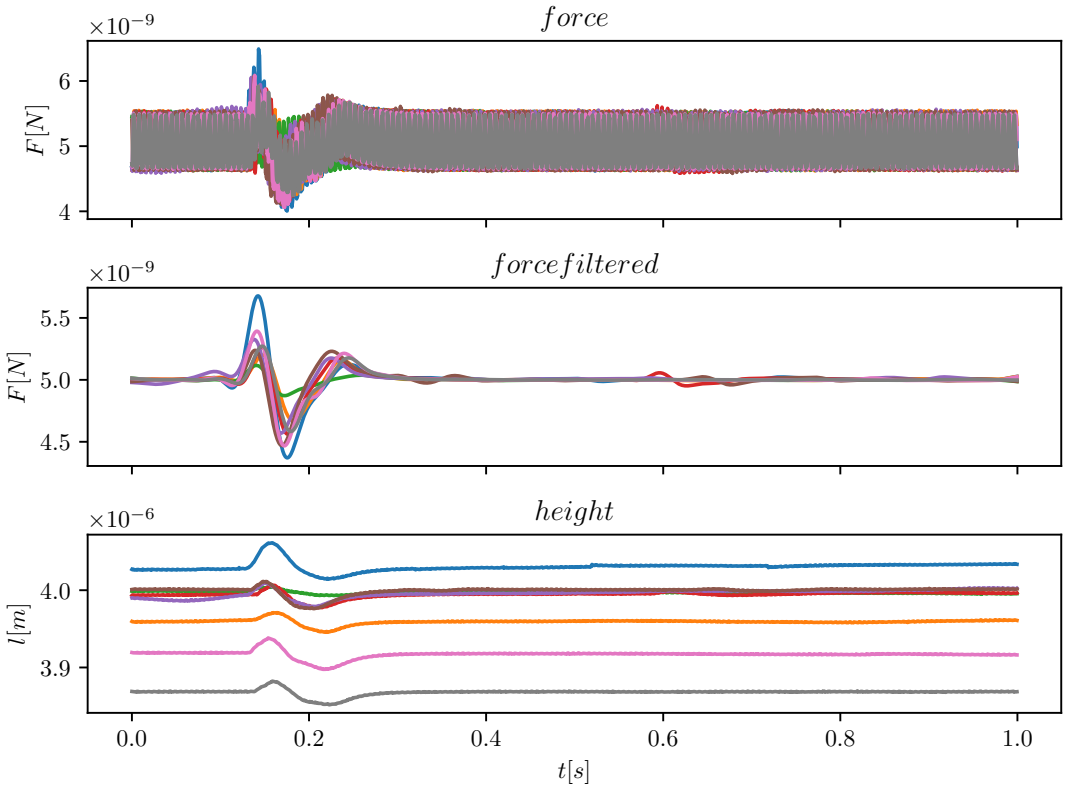

Figure 5.11: Data from AFM measurement. Eight impulses shown.

Chapter 6

Discussion

6.1 Experimental results

The first aim of this work was to measure mechanical changes of axon during the action potential. In the experiment, it was showed that the spontaneous action potentials are accompanied by a displacement of axon surface. The smallest changes of the surface displacement were measured to be 9.1 ± 3.8nm and the highest 16.9 ± 7.5nm. Tasaki measured the displacement to be in range $0.5 - 1.0$nm and Heimburg reported values around $1.2nm$ [26, 30]. The difference which might play a role is that this experiment recorded spontaneous potentials and both Tasaki and Heimburg measured evoked potentials. The mouse action potentials can be divided into short and long ones. Data from AFM also show short and long mechanical impulses. Long mechanical impulses had duration of $170 - 190$ms and the short ones had duration of 50ms. The action potentials measured at Institute of experimental Medicine have shorter lenghts (15ms and $25 - 30$ms). These data of action potentials were measured by 50pA patch-clamp technique which means they were not purely spontaneous. The work of Risner-Janiczek, 2011 reports the lengths of action potentials to be 25ms and 130ms (these values were determined from the presented graphs using the same practise employed in this work) [42].

The first issue with the experimental part is the need of transferring the cells from one workplace to another one. Even though an incubator with controlled temperature was used, the cells often seemed to be already dying. If the cells were cultivated at the faculty which posses the AFM, the problem would be solved. At the time of writing this thesis it was not possible.

Another issue is to identify axons and dendrites. The axons are the main communication channels for neurons. Especially in this stage of neural tissue development the cells fire not only single potentials but also bursts with many spikes. This means that if nothing is detected there is a chance a dendrite was measured. Cells with protein called GFP were inspected under fluorescent microscope but no criterion which would help in locating axons in cells without GFP was established. The AFM did not feature fluorescent microscope so it was impossible to measure the GFP cells directly in AFM.

The fastest potentials according to the electrical data are of duration about 15ms, or in terms of frequency 67Hz. The sampling frequency of the AFM is 2048Hz. The sampling frequency is therefore considerably higher than it needs to be. But there is another issue which affects the measurements itself. When the axon swells during the potential the membrane of the axon curves. The principle of the AFM is a cantilever touching the

axon and a laser reflecting from the cantilever to a photodiode. If the membrane curves sufficiently fast then the cantilever can be thrown off the membrane. This means that there will be no contact between the membrane and the cantilever which would result in measuring a nonsense. The AFM would measure no force at all, and this would be recorded in the data. Such severe discontinuities were measured for few impulses. It´s not known whether the cantilever does not return quickly enough or if there is another problem.

To confirm that these mechanical impulses are indeed coupled to the electrical ones it is needed to record simultaneously mechanical and electrical data. The cells can be cultivated on a modified Petri dish with integrated electrodes. The end of electrodes are placed in a grid pattern at the bottom of the Petri dish. The grid is not fine enough to monitor the electrical impulse along the axon. It is however possible to determine if the neuron body to which the axon belongs fired the potential. The Petri dish must sit in a box which processes the information coming from all electrodes. It could not be used simultaneously with the AFM as the box was simply too big and could not be redesigned at that time to fit in.

The AFM used for this measurement is the JPK Nanowizard 3. This machine can hold the force set up in the nanonewton scale [39]. For this experiment the force was set to 5nN and to 20nN. Better results were achieved with the lower force applied to the axon. The AFM is capable of scanning the surface of a cell with incredible resolution. The problem of this experiment was the fact that the action potential is a highly dynamic phenomenon. The change of height results in a very small change in force. It can be noted that the peak force is only little greater than the noise itself.

Looking at the Figure 4.5, it might seem that both axons and dendrites are stained with GFP. Inspecting the cells with a microscope, it was seen that not every neurite was glowing. At the same time there was no certainty that only the axons were coloured. This could be because of the long time before watching the cells under the microscope. The cells needed to be transported by car. Box with controlled temperature but not atmosphere was used for the transfer which could damage the cells. The proteins do not stay in the axons forever, but they are transported out of the axon membrane by various processes. Consequently not only axons are glowing, but also the cell bodies and to some extent dendrites. Because of the inability to use the fluorescent microscope directly with AFM, this technique of colouring axons was tried only few times with the nanoindenter.

6.2 Numerical results

The second aim of this work was to explain the conductance data by the behaviour of the cell membrane. This was done using the viscoelastic model to describe the behaviour of the membrane. Three viscoelastic models were derived and fitted to the conductance data of Hodgkin and Huxley. One of these models, the parallel model, was able to fit both potassium and sodium channel. The model predicts the stiffening of the membrane and low viscosity for high values of voltage.

The conductance data are the original data published by Hodgkin and Huxley from 1952. Newer and more accurate data are, of course, available. The purpose of this work was not to fit the most recent data in the best way but to show that the action potential

can be partly modeled as a mechanical phenomenon. The Hodgkin-Huxley model has undergone few changes. In much software for fitting the conductance data the constants $\alpha_n, \alpha_m, \alpha_h, \beta_n, \beta_m$ and β_h can be written as one generic equation 6.1 with six constants A, B, C, D, F, G to be determined [43]. Fitting these parameters with modern software of course improves the original Hodgkin-Huxley model. It does not bring, however, anything new to the model. Because of that the original model was used.

$$\alpha(V) = \frac{A + BV}{C + H \exp\left(\frac{D + V}{F}\right)} \tag{6.1}$$

For better results another optimization algorithm could be used. If a parameter space with reasonable bounds is needed to be searched, global algorithms such as *differential evolution* of *dual annealing* algorithms can be helpful. These algorithms were indeed tried. For every value of voltage the algorithm found satisfying set of parameters but each parameter was quiet different for each voltage. With the *curvefit* algorithm it was sufficient to take the previous parameters as initial value for another voltage. This resulted in parameters not so different for each voltage value. For potassium channel it was possible to establish a linear dependency of these parameters on voltage most parameters.

The viscoelastic model is based on the assumption that the ion channels directly participate in the stress-deformation process. In other words the deformation of ion channels has an impact on the deformation of the whole membrane. Even with many ion channels in the membrane, their area is small as the ion channels are composed by only few proteins. This raises a question whether it is appropriate to include the ion channels in the viscoelastic equation. It is possible that the mechanics of the membrane does not care about the contribution from ion channels. It does not mean ion channels cannot operate in a mechanical manner. One possibility is to exclude the ion channels from the main viscoelastic equation, compute the deformation of the membrane and afterwards compute the deformation of the ion channels from the behaviour of the membrane.

There are studies about measuring the viscosity and elasticity of a cell membrane [44, 45, 46]. The problem is that the viscoelastic models most applied for describing the membrane are the Kelvin model and Standard linear solid model [44]. The Kelvin model has two elements and Standard linear solid has three elements. The computed viscosity and elasticity of presented four element models are therefore incompatible with these measurements. Models with less than four parameters were incapable to include channel's viscosity and elasticity. The fact that Kelvin and standard linear model are the most common models does not mean it is a settled fact. For example power law models [45] or fractional models are being examined [46].

Chapter 7

Conclusion

This work presents a unique experiment with mouse nerve impulses. It was demonstrated that a viscoelastic model of the cell membrane can be used to explain change of conductance of excitable cells. It could mean the membrane is not a passive capacitor as suggested by Hodgkin and Huxley but it has active role in formation and propagation of action potential. The model predicts the stiffening of the membrane for depolarization which is in agreement with the soliton by Heimburg et al. The numerical study was complemented by experimental measurements of spontaneous action potentials. Detected signals measured by AFM indicate a link between action potential and vertical membrane deflection.

It is believed that the presented mechanics of action potential can shift the view from phenomenological models to models which acknowledges the role of excitable membrane. Understanding the link between the membrane and the action potential could result in new anesthetics based on the mechanical properties of the membrane. Another advantage of this model would be the ability to better understand action potentials in excitable cells with different membrane composition and to formulate more general conclusions about cell behaviour.

Appendix A

Protocol

Abstract This protocol describes a method for measuring nerve impulses in axons with the use of Atomic force microscopy. Neuronal tissue of mice is used. The uniqueness of the experiment is due to the fact that AFM is performing the measurement on the living neurons which are in no case electrically stimulated. This enables to study the true progression of mechanical phenomena during the nerve impulses.

Part of this protocol deals with the preparing and cultivating the spinal neurons. This is performed at the Institute of Experimental Medicine, Czech Academy of Sciences. The protocol for the cultivation is yet unpublished. The description here is not considered to provide a complete guideline on how to prepare the cells, rather to present an overview of such preparation.

Materials for cell cultures

- Hibernate-E (Gibco, Thermo Fisher)
- 0.8% BSA (Sigma-Aldrich)
- 0.4% BSA (Sigma-Aldrich)
- DNase (Sigma-Aldrich)
- 50% DMEM, low glucose (Gibco, Thermo Fisher)
- 25% Horse serum (Gibco, Thermo Fisher)
- 25% HBSS without Ca2+ or Mg2+ (Gibco, Thermo Fisher)
- 1% Penicillin-Streptomycin (Gibco, Thermo Fisher)
- MACS Neuro Medium (Miltenyi Biotech)
- 2% NeuroBrew 21 (Miltenyi Biotech)
- 1% Glutamax (Thermo Fisher)
- 1% ITS+ (Sigma-Aldrich)

Equipment for measuring

- JPK Instruments Nanowizard 3 microscope
- AppNano HYDRA6V-200NG-SiO2-5 probe
- AppNano HYDRA6V-200NG-TL cantilever
- Panasonic Biomedical MCO-5M-PE incubator

Procedure

- Prepare all mediums needed for cell culture as described in Box 1
- Isolate cells as described in Box 2
- Setup AFM for measurement as described in box 3
- Prepare cells for measuring described in Box 4
- Select suitable axon and perform measurement as described in Box 5

BOX 1 | Preparing the mediums

Four mediums are needed for the process of isolating the cells, Disruption medium 1 - DM1, Disruption medium 2 - DM2, Plating medium - PM and Cultivation medium - CM.

1. DM1 consists of Hibernate-E, 0.8% BSA and 100µg/ml DNase. The approximate total volume is 1ml.
2. DM2 consists Hibernate-E, of 0.4% BSA, 20µm/ml DNase and 50% DMEM, low glucose. The approximate total volume is 2ml.
3. PM consists of 25% Horse serum (Gibco, Thermo Fisher), 25% HBSS without Ca2+ or Mg2+, 1% Penicillin-Streptomycin (10,000 U/mL), MACS Neuro Medium and 2% NeuroBrew 21. The approximate total volume is 30ml.
4. CM consists of 1% Glutamax, 1% ITS+ and 1% Penicillin-Streptomycin. The approximate total volume is 50ml.

BOX 2 | Isolation of the cells

Spinal neurons are isolated from E13.5-E14.5 embryos from C57BL/6J mice.

1. Extract the spinal cords from embryos and immerse them in cold Hibernate-E medium. Remove the meninges and store the tissue on ice in Hibernate-E.
2. Wash the tissue with 1ml of HBSS, without Ca2+ or Mg2+ two times. Digest the tissue in papain-based Neuron Isolation Enzyme (Thermo Scientific Pierce) by adding 30ul of enzyme solution per 1 spinal cord for 9min at 37°C. Carefully remove the enzyme and place the tissue in DM1.
3. Disrupt the tissue by trituration with P1000 tip gently a few times and leave it to settle for 2min. Transfer the supernatant to a new tube, while triturating the tissue pellet again in DM2. Repeat this step once more if any tissue fragments remains after second disruption. Transfer the supernatant containing disrupted tissue by polished Pasteur pipette into a new falcon tube through a 40µm cell strainer to remove undisrupted tissue fragments. Add PM in 1:1 ratio to the filtered solution containing the cells.
4. Centrifuge the cell suspension for 5 min at 90g at 37°C, remove the supernatant and resuspend the pellet in 2ml of PM.
5. Count the cells (approximate expected amount is 1.2 million cells per spinal cord) and place them on glass coverslips coated with 100ug/ml poly-D-lysine (Thermo FIsher).

The glass coverslips are glued to a Petri dish by silica gel. Approximate number of cells cultivated in the Petri dish is about 400 000 cells. After 1h, most of the cells adhere to the coverslips, and cultivation medium (CM) was added to the plating media in 1:1 proportion. Culture is maintained by exchanging half of the media volume every 2 days. CM with ITS+ supplement is used for the first 7 days of culture, after which it is substituted for CM without ITS+ to limit proliferation of glia. Longest maintained culture was 72 days after plating.

BOX 3 | Setting up the AFM

The AppNano HYDRA6V-200NG-SiO2-5 probe is used together with HYDRA6V-200NG-TL cantilever. The probe has ball shape with radius approximately $5,2\mu m$. The AFM works in contact mode, specifically the force mode. The applied force by cantilever is $5nN$.

1. Calibrate the cantilever spring constant. The spring constant is determined by its resonance frequency. The constant should be about $0,03N/m$
2. Calibrate the cantilever sensitivity. The sensitivity is determined by indentation in a rigid body. The glass Petri dish can be used. The constant should be about $60 - 80nm/V$.
3. Setup the measuring itself. The measurement consists of three phases, *extend*, *pause* and *extract*. The *extend* and *extract* phases last $0,5s$. The *pause* phase lasts $1200s$. During the *extract* phase the cantilever approaches the neuron until the desired force is obtained. During the *pause* phase the cantilever maintains the set force. In the final phase the cantilever is lifted up.

BOX 4 | Preparing cells for measurement

Cells are stored in multigas incubator with temperature 37°C and concentration 5% CO. The Panasonic Biomedical MCO-5M-PE incubator is used. The cells should be in the incubator at least half an hour in order to stabilize the teperature of cells.

1. Put glass with cells to a Petri dish. Add medium so that the Petri dish is filled at least to 5mm from bottom. If the cantilever exits the liquid, the laser reflection will change dramatically during measurement. This is unwanted behaviour. The medium must have the same temperature as the cells.
2. Put the Petri dish in the AFM.
3. Lower the cantilever so that it is immersed in the medium.
4. Calibrate the laser. The laser should point to the centre of the photodiode.

Warning The cells should be inspected before the first measurement and also after every measurement. The cells should look elongated. If the cells are round it is an indication that the cells are dying.

BOX 5 | Measuring the cells

Measurement of cells is performed at a laboratory which has temperature 24°C. Highest neural activity of cells is at temperature around 37°C. One measurement takes 20 minutes. Two measurements are performed on one cell culture. The measurement is not performed twice on the same spot.

1. Select suitable axon. The axon should be long and not branch to multiple others.

2. Navigate the cantilever to the selected axon. Lower the cantilever so that it is in contact with the axon.

Caution If the axon is thin, it is possible that the tip falls off from axon. It is better to choose axons with larger diameter. As the axons are not rigidly connected to the Petri dish, the cantilever can shift the axon from its initial position. Lastly, the tip of the cantilever can pierce the axon. It is necessary to inspect the condition of the axon after each measurement visually.

Bibliography

[1] A. Jerusalem, Z. Al-Rekabi, H. Chen, A. Ercole, M. Malboubi, M. Tamayo-Elizalde, L. Verhagen, and S. Contera, "Electrophysiological-mechanical coupling in the neuronal membrane and its role in ultrasound neuromodulation and general anaesthesia," *Acta Biomaterialia*, vol. 97, pp. 116–140, 2019.

[2] I. Tasaki and P. Byrne, "Volume expansion of nonmyelinated nerve fibers during impulse conduction.," *Biophysical Journal*, vol. 57, no. 3, p. 633, 1990.

[3] G. Kim, P. Kosterin, A. Obaid, and B. Salzberg, "A mechanical spike accompanies the action potential in mammalian nerve terminals," *Biophysical Journal*, vol. 92, no. 9, pp. 3122–3129, 2007.

[4] C. Fillafer, M. Mussel, J. Muchowski, and M. F. Schneider, "Cell surface deformation during an action potential," *Biophysical Journal*, vol. 114, no. 2, pp. 410–418, 2018.

[5] K. Franze, "The mechanical control of nervous system development," *Development*, vol. 140, no. 15, pp. 3069–3077, 2013.

[6] J. G. Nicholls, A. R. Martin, B. G. Wallace, and P. A. Fuchs, *From neuron to brain*, vol. 271. Sinauer Associates Sunderland, MA, 2001.

[7] A. L. Hodgkin, A. F. Huxley, and B. Katz, "Measurement of current-voltage relations in the membrane of the giant axon of loligo," *The Journal of physiology*, vol. 116, no. 4, pp. 424–448, 1952.

[8] W. contributors, "Schematic of an action potential." `https://en.wikipedia.org/wiki/Action_potential#/media/File:Action_potential.svg`, 2007. Online; accessed 4-August-2021.

[9] J. Bernstein, "Untersuchungen zur thermodynamik der bioelektrischen ströme," *Archiv für die gesamte Physiologie des Menschen und der Tiere*, vol. 92, no. 10, pp. 521–562, 1902.

[10] A. L. Hodgkin and B. Katz, "The effect of sodium ions on the electrical activity of the giant axon of the squid," *The Journal of physiology*, vol. 108, no. 1, pp. 37–77, 1949.

[11] L. Abbott, "Lapicque's introduction of the integrate-and-fire model neuron (1907)," *Brain Research Bulletin*, vol. 50, pp. 303–304, 1999.

[12] A. Hodgkin and A. Huxley, "A quantitative description of membrane current and its application to conduction and excitation in nerve," *The Journal of Physiology*, vol. 117, pp. 500–544, 1952.

[13] W. contributors, "Cable theory — Wikipedia, the free encyclopedia." `https://en.wikipedia.org/w/index.php?title=Cable_theory&oldid=1015853177`, 2021. Online; accessed 4-August-2021.

[14] J. Nagumo, S. Arimoto, and S. Yoshizawa, "An active pulse transmission line simulating nerve axon," *Proceedings of the IRE*, vol. 50, pp. 2061–2070, 1962.

[15] E. Wilke, "Das problem der reizleitung im nerven vom standpunkte der wellenlehre aus betrachtet," *Pflüger's Archiv für die gesamte Physiologie des Menschen und der Tiere*, vol. 144, no. 1, pp. 35–38, 1912.

[16] A. El Hady and B. B. Machta, "Mechanical surface waves accompany action potential propagation," *Nature Communications*, vol. 6, no. 1, pp. 1–7, 2015.

[17] T. Heimburg and A. D. Jackson, "On soliton propagation in biomembranes and nerves," *Proceedings of the National Academy of Sciences*, vol. 102, no. 28, pp. 9790–9795, 2005.

[18] M. Mussel and M. F. Schneider, "It sounds like an action potential: unification of electrical, chemical and mechanical aspects of acoustic pulses in lipids," *Journal of The Royal Society Interface*, vol. 16, no. 151, p. 20180743, 2019.

[19] J. Engelbrecht, T. Peets, K. Tamm, M. Laasmaa, and M. Vendelin, "On the complexity of signal propagation in nerve fibres.," *Proceedings of the Estonian Academy of Sciences*, vol. 67, no. 1, 2018.

[20] M. Heinricher, "Principles of extracellular single-unit recording," in *Microelectrode Recording in Movement Disorder Surgery* (K. J. Israel, Zvi; Burchiel, ed.), 2004.

[21] L. Molecular Devices, *Axon guide : a guide to electrophysiology and biophysics laboratory techniques*. MDS Analytical Technologies, California, United States, 2012.

[22] J. W. Moore, "Voltage clamp," *Scholarpedia*, vol. 2, no. 9, p. 3060, 2007.

[23] A. C. Daly, D. Gavaghan, C. Holmes, and J. Cooper, "Hodgkin–Huxley revisited: reparametrization and identifiability analysis of the classic action potential model with approximate Bayesian methods," *Royal Society Open Science*, vol. 2, 2015.

[24] D. Hill, "The volume change resulting from stimulation of a giant nerve fibre," *The Journal of Physiology*, vol. 111, no. 3-4, pp. 304–327, 1950.

[25] T. Heimburg, *Thermal biophysics of membranes*. John Wiley & Sons, 2008.

[26] I. Tasaki and K. Iwasa, "Rapid pressure changes and surface displacements in the squid giant axon associated with production of action potentials," *The Japanese journal of Physiology*, vol. 32, no. 1, pp. 69–81, 1982.

[27] S. Terakawa, "Potential-dependent variations of the intracellular pressure in the intracellularly perfused squid giant axon.," *The Journal of Physiology*, vol. 369, no. 1, pp. 229–248, 1985.

[28] B. Abbott, J. Howarth, and J. Ritchie, "The initial heat production associated with the nerve impulse in crustacean and mammalian non-myelinated nerve fibres," *The Journal of Physiology*, vol. 178, no. 2, p. 368, 1965.

[29] J. Ritchie and R. Keynes, "The production and absorption of heat associated with electrical activity in nerve and electric organ," *Quarterly Reviews of Biophysics*, vol. 18, no. 4, pp. 451–476, 1985.

[30] A. Gonzalez-Perez, L. D. Mosgaard, R. Budvytyte, E. Villagran-Vargas, A. D. Jackson, and T. Heimburg, "Solitary electromechanical pulses in lobster neurons," *Biophysical Chemistry*, vol. 216, pp. 51–59, 2016.

[31] M. D. Forrest, "Can the thermodynamic hodgkin-huxley model of voltage-dependent conductance extrapolate for temperature?," *Computation*, vol. 2, no. 2, pp. 47–60, 2014.

[32] S. J. Singer and G. L. Nicolson, "The fluid mosaic model of the structure of cell membranes," *Science*, vol. 175, no. 4023, pp. 720–731, 1972.

[33] H. Barz, A. Schreiber, and U. Barz, "Impulses and pressure waves cause excitement and conduction in the nervous system," *Medical Hypotheses*, vol. 81, no. 5, pp. 768–772, 2013.

[34] W. Flügge, *Viscoelasticity*. Springer Science & Business Media, 2013.

[35] J. Furmanski, L. A. Pruitt, L. A. Pruitt, and A. M. Chakravartula, *Viscoelasticity*, p. 208–240. Cambridge University Press, 2011.

[36] P. Virtanen, R. Gommers, T. E. Oliphant, M. Haberland, T. Reddy, D. Cournapeau, E. Burovski, P. Peterson, W. Weckesser, J. Bright, S. J. van der Walt, M. Brett, J. Wilson, K. J. Millman, N. Mayorov, A. R. J. Nelson, E. Jones, R. Kern, E. Larson, C. J. Carey, İ. Polat, Y. Feng, E. W. Moore, J. VanderPlas, D. Laxalde, J. Perktold, R. Cimrman, I. Henriksen, E. A. Quintero, C. R. Harris, A. M. Archibald, A. H. Ribeiro, F. Pedregosa, P. van Mulbregt, and SciPy 1.0 Contributors, "SciPy 1.0: Fundamental Algorithms for Scientific Computing in Python," *Nature Methods*, vol. 17, pp. 261–272, 2020.

[37] L. F. Shampine and S. Thompson, "Stiff systems," *Scholarpedia*, vol. 2, no. 3, p. 2855, 2007.

[38] P. C. Braga and D. Ricci, eds., *Atomic force microscopy: biomedical methods and applications*, vol. 242. Springer Science & Business Media, 2004.

[39] J. I. team, *The NanoWizard AFM handbook*. Bruker Nano Surfaces division, Berlin, Germany, 2005.

[40] N. n. Emily Maetz, "Atomic force microscope illustration." `https://www.nisenet.org/catalog/scientific-image-atomic-force-microscope-illustration`, 2016. Online; accessed 6-August-2021.

[41] K. Holthoff, Y. Kovalchuk, and A. Konnerth, "Dendritic spikes and activity-dependent synaptic plasticity," *Cell and tissue research*, vol. 326, no. 2, pp. 369–377, 2006.

[42] J. R. Risner-Janiczek, M. A. Ungless, and M. Li, "Electrophysiological properties of embryonic stem cell-derived neurons," *PLoS One*, vol. 6, no. 8, p. e24169, 2011.

[43] S. S. Steven H. Koslow, ed., *Databasing the Brain: From Data to Knowledge*. Wiley, New York, 2004.

[44] H. Aghaie, M. Saghafian, and D. Saeidi, "Elastic and viscoelastic modeling of cell deformation in acoustically driven microchannel.," *Journal of Applied Fluid Mechanics*, vol. 13, no. 6, 2020.

[45] J. Gounley and Y. Peng, "Computational modeling of membrane viscosity of red blood cells," *Communications in Computational Physics*, vol. 17, no. 4, pp. 1073–1087, 2015.

[46] D. Craiem and R. L. Magin, "Fractional order models of viscoelasticity as an alternative in the analysis of red blood cell (rbc) membrane mechanics," *Physical Biology*, vol. 7, no. 1, p. 013001, 2010.